GEORG-AUGUST-UNIVERSITÄT
GÖTTINGEN

Fakultät für
Physik

Bachelor's Thesis

Neutrino-Rekonstruktion mit KLFitter

Neutrino Reconstruction with KLFitter

prepared by

Marie Reinecke

from Alfeld (Leine)

at the II. Physikalischen Institut

Thesis number: II.Physik-UniGö-BSc-2015/14

Thesis period: 24th April 2015 until 30th July 2015

First referee: Prof. Dr. Arnulf Quadt

Second referee: Prof. Dr. Ariane Frey

Abstract

When a pair of a top and an antitop quark decays semileptonically, it produces two bottom quark jets, two jets from lighter quarks, a charged lepton and a neutrino in the end. The charged lepton's signal can be easily identified as lepton but the four jet signals cannot be assigned to the different quarks of the decay so easily. In addition, the neutrino cannot be observed at all. For this, the Kinematic Likelihood Fitter (KLFitter) was developed to find the most likely assignment of the jet signals to the quarks. Also, via using the well-known masses of top quark and W-boson the lepton and the neutrino are reconstructed.

The x- and y-components of the neutrino momentum can be reconstructed directly via $E_{\mathrm{T}}^{\mathrm{miss}}$ while p_z is calculated from the mass of the W-boson. But the reconstruction efficiency is relatively low.

In this bachelor thesis, attempts to improve this reconstruction efficiency are made by analysing the code of KLFitter and the efficiency checking algorithm. With newly implemented changes in both frameworks the efficiency for the neutrino can be raised to almost 25 % involving slight improvements for the other decay particles and an improvement from about 45 % to about 50 % for the leptonic top quark.

Zusammenfassung

Beim semileptonischen Zerfall eines Teilchenpaares aus Top- und Antitop-Quark entstehen zwei Bottom-Quark-Jets, zwei Jets aus leichteren Quarks, ein geladenes Lepton und ein Neutrino. Das Signal des geladenen Leptons kann leicht als geladenes Lepton identifiziert werden, während die vier Jets nicht so einfach den Quarks des Zerfalls zugeordnet werden können. Eine weitere Unsicherheit ist das Neutrino, das überhaupt nicht beobachtet werden kann. Daher wurde der Kinematic Likelihood Fitter (KLFitter) entwickelt, der die wahrscheinlichste Zuordnung zwischen den Jet-Signalen und den Quarks im Zerfall findet. Des Weiteren werden über die gut bekannten Massen des Top-Quarks und des W-Bosons die Signale des geladenen Leptons und des Neutrinos bestimmt.

Die x- und y-Komponente des Neutrinoimpulses können direkt über $E_{\mathrm{T}}^{\mathrm{miss}}$ berechnet werden, während p_z über die Masse des W-Bosons berechnet wird. Die Rekonstruktionseffizienz ist dennoch vergleichsweise niedrig.

In dieser Bachelorarbeit werden Ansätze zur Verbesserung der Neutrino-Rekonstruktionseffizienz dargestellt. Dafür wird der Programmcode von KLFitter und der die Effizienz von KLFitter bestimmende Algorithmus analysiert. Mit neu implementierten Änderungen in beiden Programmen wird die Effizienz für das Neutrino auf fast 25 % angehoben, was auch eine leichte Verbesserung aller anderen Teilchen des Zerfalls bewirkt. Für das leptonisch zerfallende Top-Quark verbessert sich die Rekonstruktionseffizienz von etwa 45 % auf etwa 50 %.

Contents

Nomenclature

Latin Letters

Variable	Meaning	Unit
$\mathcal{B}$	branching fraction	
c	speed of light	$^{\mathrm{m}}/_{\mathrm{s}}$
E	energy	GeV
p	momentum	$^{\mathrm{GeV}}/_{\mathrm{c}}$
m	mass	$\frac{\mathrm{GeV}}{c^2}$
$\sqrt{s}$	centre-of-mass energy	GeV

Greek Letters

Variable	Meaning	Unit
τ	lifetime	s
τ_{had}	hadronization time	s
α	fine-structure constant	
α_s	strong coupling constant	
θ_W	Weinberg angle, $\sin^2\theta_W \approx 0.23$	

Indices

Index	Meaning
ℓ	lepton
ν	neutrino
T	transverse, in the x-y-plane
x	in x-direction in right-handed coordinates
y	in y-direction in right-handed coordinates

Index	**Meaning**
z	in z-direction in right-handed coordinates
true	true
reco	reconstructed
miss	missing
meas	measured
had	hadronic
lep	leptonic
alljet	all-jets decay channel
dilep	dileptonic decay channel
semilep	semileptonic decay channel

1. Introduction

The experiments of ATLAS and CMS have been all over the media since the start of the LHC collider at CERN in Geneva. This is because they are the largest two detectors of the world's most powerful particle accelerator. It can accelerate protons so that they circle $11,245$ times per second around the 27 km long beam pipe. Then, these proton bunches are collided at very high energies and very small scales. The LHC is in many aspects the most extreme machine that humanity has created yet. Considering this, it is no wonder people are fascinated by it and the research it involves. For example, the most recent event that generated a lot of media attention was the discovery of the Higgs boson.

Another important object of investigation is the top quark. As heaviest of all quarks, it decays before it can even form bound states. Therefore, it can be observed in a detector only by its decay products. One possibility of this is the semileptonic decay channel where the pair of a top and an antitop quark both decay into a (anti)bottom quark and a W-boson. One of the W-bosons decays into a charged lepton and a neutrino while the other one decays into two lighter quarks.

To support analyses regarding the top quark properties, the Kinematic Likelihood Fitter (KLFitter) was developed. It reconstructs the most probably correct assignment of jets to partons out of detector signals of particular decay channels. In this thesis, the reconstruction efficiency of the neutrino in the semileptonic decay channel will be discussed.

To prepare the analysis, the following chapter presents the Standard Model of Particle Physics and focuses especially on the top quark. The third chapter explains the proton-proton collider LHC and in particular the ATLAS detector that is important for the studies connected to this thesis. After that, the used programs, the KLFitter and the MatchMonster framework, are introduced. This is followed by a chapter about the results of all attempts on increasing the neutrino reconstruction efficiency in analyses with KLFitter. In this context, the quality of the results is also discussed. Lastly, the conclusion and a brief outlook on future studies on this topic are given.

2. The Standard Model and the Top Quark

This chapter includes a short introduction into the theoretical background of the Standard Model of Particle Physics. After that, it focuses on the main subject of this thesis, the production and decay of the top quark and especially the decay of top-antitop pairs.

2.1. The Standard Model of Particle Physics

Based on the theory of the Electroweak Unification by Glashow, Salam and Weinberg, the Standard Model of Particle Physics was developed in the 1960s and 1970s. Its second basic module is the Quantum Chromodynamics (QCD) so that the Standard Model is able to describe the behaviour of the particles around us as well as their interactions very precisely [1–11].

Still, the Standard Model is not suitable to be a Theory of Everything since there are a few observed things that cannot be explained or gaps are existing in this context. The past main problem that was just recently solved by the discovery of the Higgs boson at the LHC [12, 13] was that the observed particles have a mass even though there is no reason in the Standard Model for massive particles.

Now, the remaining questions are for example how the different masses of the particles are calculated. Many other values are also only taken from experiment and validated by testing if it fits into the context of the Standard Model theories. This makes at least 18 free parameters that form the Standard Model according to the experimental needs. Another few of the remaining questions are: Is there a unification of the strong and electroweak force? What about gravitation? What kind of particles does dark matter consist of? So there is much further research needed [14, 15].

2.1.1. Quarks, Leptons and Bosons

There are three types of elementary particles known at the moment that matter is made of. Those are called leptons, quarks and bosons. The latter are subject to the next

chapter.

Leptons and quarks are comprised into the term *fermions*, which describes particles with a half-integral spin value. Both of these are divided into three generations. For the leptons, the first generation contains the electron e and the electron neutrino ν_e, the second generation is formed by the muon μ and its neutrino ν_μ and the last one is the tau τ with the tau neutrino ν_τ. The quarks can be separated into up-type (up u, charm c, top t) and down-type quarks (down d, strange s, bottom b) where the first quarks up and down form the first generation and so on. The higher the number of the generation, the higher is the quark's mass. All fermion masses are listed in Table 2.1. In Table 2.2 other useful properties of fermions are listed [14]. As neutrinos are always left-handed and antineutrinos right-handed there is no right-handed value for these in the columns of T_3 and Y.

Quarks	Mass $m\,[\mathrm{MeV}/c^2]$	Leptons	Mass $m\,[\mathrm{MeV}/c^2]$
u	$2.3^{+0.7}_{-0.5}$	e	$0.510998928 \pm 0.000000011$
d	$4.8^{+0.5}_{-0.3}$	μ	$105.6583715 \pm 0.0000035$
c	$1,275 \pm 25$	τ	1776.82 ± 0.16
s	95 ± 5	ν_e	$< 2 \cdot 10^{-6}$
t	$173,210 \pm 510 \pm 710$	ν_μ	$< 2 \cdot 10^{-6}$
b	4180 ± 30	ν_τ	$< 2 \cdot 10^{-6}$

Table 2.1.: The fermion masses as defined by the currently best measurements [16].

Particle Type	Generation 1	2	3	$Q\,[e]$	C	T_3 L	T_3 R	Y L	Y R
Leptons	ν_e	ν_μ	ν_τ	0	none	$+\frac{1}{2}$	-	-1	-
	e	μ	τ	-1	none	$-\frac{1}{2}$	0	-1	-2
Quarks	u	c	t	$+\frac{2}{3}$	r,g,b	$+\frac{1}{2}$	0	$+\frac{1}{3}$	$+\frac{4}{3}$
	d	s	b	$-\frac{1}{3}$	r,g,b	$-\frac{1}{2}$	0	$+\frac{1}{3}$	$-\frac{2}{3}$

Table 2.2.: List of properties of the fermions in the Standard Model. Given properties are the electric charge Q, the colour charge C, the third component of the weak isospin T and the weak hypercharge calculated by $Y = 2\,(Q - T_3)$. For the last two values, the particles need to be separated into left-handed ($_\mathrm{L}$) and right-handed ($_\mathrm{R}$). The here mentioned down-type quarks d, s and b are the electroweak eigenstates and not the mass eigenstates that the electroweak ones are linear combinations of. For all these details of the electroweak interaction see Section 2.1.2 [14, 15, 17].

2.1.2. Interactions

The Standard Model includes three elementary interactions between matter. Those are the electromagnetic force mediated by the photon, the strong force mediated by gluons and the weak interaction that is mediated either by the Z or a charged W. Another elementary interaction is gravitation. This fourth force is left out here because it cannot yet be described by the Standard Model and its assumed mediator called the graviton has not been proven to even exist. All forces' mediators are also called *bosons* which is the term for particles with an integral spin. Another boson is the recently discovered Higgs particle H^0 which is the observed excitation of the Higgs field that gives other particles its mass. Other than the gauge bosons that all have a spin of $s = 1$, the Higgs boson has spin 0. Other properties of the bosons are listed in Table 2.3.

Force	Boson	Mass m [GeV/c^2]	Q [e]	T_3	Gauge Coupling g
Electromagnetic	Photon γ	$0(< 1 \cdot 10^{-27})$	0	0	$\sqrt{4\pi\alpha}$
Strong	Gluon g	0	0	0	$\sqrt{4\pi\alpha_s}$
Weak	Z^0	91.1876 ± 0.0021	0	0	$\sqrt{4\pi\alpha}/\left(\sin\theta_W \cos\theta_W\right)$
Weak	$W^\pm$	80.385 ± 0.015	± 1	± 1	$\sqrt{4\pi\alpha}/\sin\theta_W$
-	H^0	127.7 ± 0.4	0	0	- (no gauge boson)

Table 2.3.: List of properties of the bosons in the Standard Model. Given properties are the mass m, the electric charge Q the third component of the weak isospin T_3 and the strength of the gauge coupling g [16].

Each of the forces is described by a physical theory. These theories are called *Quantum Electrodynamics (QED)* for the electromagnetic force, *Quantum Chromodynamics (QCD)* for the strong force and the *Glashow-Weinberg-Salam (GWS) theory* not only for the weak force but already for a so-called electroweak force where the weak and the electromagnetic force are two aspects of this single theory.

Because the Standard Model is a gauge theory the interactions are described by local gauge symmetries and their gauge groups. This is for the electromagnetic force the group $\mathrm{U(1)_{EM}}$ with the transformation $\phi \rightarrow \phi' = \exp(i\theta)\phi$, where ϕ is a spinor field and θ is a real number. The symmetry group $\mathrm{SU(3)}_C$ describes all QCD relations (C stands for colour charge). It contains the Gell-Mann matrices λ_k with $k = 1, ..., 8$. As these each stand for one gluon, this is the reason why there are eight differently colour charged gluons, each carrying a colour and an anticolour of (anti)red, (anti)blue and (anti)green.

Because of their own charge, gluons can couple to each other and therefore do not exist as single particles. Another reason for this is the quark confinement that originates from the appearance of quark-antiquark pairs at the separation of two initial quarks.

Also quarks cannot exist by themselves but always form colour neutral bound states that also have an electromagnetic charge of an integer value.

The weak force is described by the symmetry group SU(2) with three Pauli matrices σ_i, with $i = 1, 2, 3$. With this the electroweak symmetry is unified to the symmetry group $\mathrm{SU(2)_L} \otimes \mathrm{U(1)}_Y$. The index L is chosen because the weak isospin current T only couples to left-handed fermions. Y stands for the weak hypercharge that is listed in Table 2.2 as $Y = 2\,(Q - T_3)$. For explanations of all these values and contexts see the next paragraph [14].

Combining all these theories gives the *Standard Model Symmetry Group*

$$\mathrm{SU(3)}_C \otimes \mathrm{SU(2)_L} \otimes \mathrm{U(1)}_Y.$$

Electroweak Interaction

While the strong and electromagnetic force couple between particles that carry the corresponding colour charge or electric charge, the weak force carriers couple to all fermions (and in rare cases to each other and other bosons).

There are two types of weak interactions. The first one is the *neutral current* that gets its name because it is mediated by the Z^0-boson which has no electric charge. The gauge boson of the *charged current* is the W^+ or W^--boson. Only the latter, the charged weak interaction, can change the *flavour* of a particle (simply put, every fermion has a different flavour), for example let an electron convert into an electron neutrino ν_e under emission of a W^- or absorption of a W^+. For quarks, the weak force can even act between the generations. The reason is that the quark generations are rotated for this interaction. That means instead of coupling the physical quarks like

$$\begin{pmatrix} u \\ d \end{pmatrix}, \begin{pmatrix} c \\ s \end{pmatrix}, \begin{pmatrix} t \\ b \end{pmatrix},$$

it couples pairs of

$$\begin{pmatrix} u \\ d' \end{pmatrix}, \begin{pmatrix} c \\ s' \end{pmatrix}, \begin{pmatrix} t \\ b' \end{pmatrix},$$

where d', s' and b' are not the physical quarks but linear combinations of them that are

specified by the *Cabibbo-Kobayashi-Maskawa (CKM) matrix*

$$\begin{pmatrix} d' \\ s' \\ b' \end{pmatrix} = \begin{pmatrix} V_{ud} & V_{us} & V_{ub} \\ V_{cd} & V_{cs} & V_{cb} \\ V_{td} & V_{ts} & V_{tb} \end{pmatrix} \begin{pmatrix} d \\ s \\ b \end{pmatrix}.$$

The matrix can be reduced down to four independent parameters - three real numbers and a complex phase factor. This phase factor is the reason why the weak force violates the conservation of charge and parity (CP-violation) [14, 17].

The values of the different matrix elements are not given by theory but were identified from experiments [16]:

$$\begin{pmatrix} 0.97427 \pm 0.00014 & 0.22536 \pm 0.00061 & 0.00355 \pm 0.00015 \\ 0.22522 \pm 0.00061 & 0.97343 \pm 0.00015 & 0.0414 \pm 0.0012 \\ 0.00888^{+0.00033}_{-0.00032} & 0.0405^{+0.0011}_{-0.0012} & 0.99914 \pm 0.00005 \end{pmatrix}.$$

Another odd circumstance is that the $W^{\pm}$ couples only to left-handed particles and right-handed antiparticles so that for the unified theory of electroweak interaction another quantum number, the weak isospin T (where T_3 is the third component of) is needed. It is different for left- and right-handed particles. Also the value of the weak hypercharge $Y = 2(Q - T_3)$ is used in this context.

2.2. The Top Quark

The first theoretical appearance of the top quark was in 1973 when Kobayashi and Maskawa proposed a third generation of quarks to fix the explanation of CP-violation in the use of weak interactions [18]. The discovery of $t\bar{t}$ pairs then happened 22 years later in $p\bar{p}$ collisions at the Tevatron Run I at $\sqrt{s} = 1.8\,\text{TeV}$ [19, 20]. Also the single top production was first discovered there in 2009 at Tevatron Run II at $\sqrt{s} = 1.96\,\text{TeV}$ [21, 22].

The top quark is an important object of research since it is the only quark that decays before it can hadronize due to its large mass and short lifetime. Hence, no hadron does exist that has a top quark as component.

Here, the important particle properties as well as the production and decay of the heaviest of quarks are presented.

2.2.1. Top Quark Properties

The most recent and exact value for the mass of the top quark is [23]

$$m_t = 173.34 \pm 0.27\,(\text{stat}) \pm 0.71\,(\text{syst})\,\text{GeV} \tag{2.1}$$

with a total uncertainty of 0.76 GeV. The relative uncertainty is of a small value of 0.44 %. The mass value combines measurements of the TEVATRON experiments CDF and DØ and the LHC Run I data of the experiments ATLAS and CMS.

The top quark is a fermion which means that it carries a spin of $s = \frac{1}{2}$. As an up-type quark, its electromagnetic charge is $Q = +\frac{2}{3}\,[e]$. But these values could not yet be measured before the top quark's decay. The reason is the predicted extremely short lifetime of

$$\tau_t = \frac{\hbar}{\Gamma_t} = 3.29 \cdot 10^{-25}\,\text{s}$$

that was calculated using the value of $\hbar = 6.58211928(15) \cdot 10^{-16}\,\text{eV s}$ [24] and the decay width of the top quark [25]

$$\Gamma_t = 2.00^{+0.47}_{-0.43}\,\text{GeV}.$$

This lifetime is much smaller than the time a top quark needs to form hadrons [26]

$$\tau_{\text{had}} = \frac{\hbar}{\Lambda_{QCD}} = \frac{\hbar}{213\,\text{MeV}} \approx 3 \cdot 10^{-24}\,\text{s}.$$

Therefore no hadrons containing any top or antitop quark do exist. Here Λ_{QCD} is the QCD scale.

2.2.2. Top Quark Production

Top quarks can be produced at hadron colliders directly in two different ways - either as top-antitop pair $t\bar{t}$ via the strong interaction or as single top quark with the contribution of the weak interaction in form of a W-boson.

$t\bar{t}$ Pair Production

As shown in Fig. 2.1, the production of $t\bar{t}$ pairs happens either if a quark and an antiquark annihilate into a gluon or if two gluons fuse.

Which of the two processes is dominant in production depends on the kind of collided

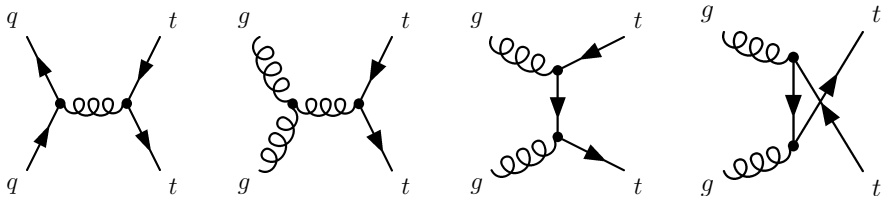

Figure 2.1.: Feynman diagrams of annihilation and gg fusion that produce $t\bar{t}$ pairs in hadron collisions.

particles ($p\bar{p}$ or pp) and the used centre-of-mass energy $\sqrt{s}$. The first defines the valence quarks and may suppress processes that need antiparticles at lower energies when only protons are available. The latter defines the parton distribution function that describes the distribution of sea quarks and gluons inside the hadrons and defines the fraction of the total momentum that a single parton holds. This controls the collision probability of each parton and gives the preferred process of $t\bar{t}$ production [27]. At TEVATRON Run II ($\sqrt{s} = 1.96\,\text{TeV}$, $p\bar{p}$) only 15 % of the production of $t\bar{t}$ pairs were initiated by gluon fusion. A different number is valid at the LHC. Here the gluons provide the dominant process with a contribution of 80 % at Run I with $\sqrt{s} = 7\,\text{TeV}$ and 90 % at Run II with $\sqrt{s} = 14\,\text{TeV}$ [16, 28].

Single Top Production

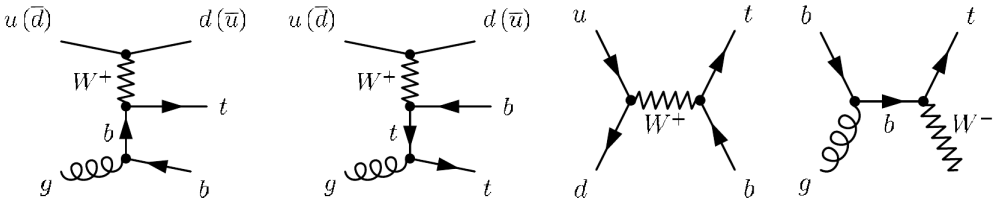

Figure 2.2.: Feynman diagrams of the leading order for the production of single top quarks in hadron collisions. The first two diagrams show examples for the t-channel while the last two show examples how the s-channel could be realized.

The second possibility to detect top quarks in hadron collisions are single quarks as produced by processes like the examples in Fig. 2.2.

These are not as easy to identify as $t\bar{t}$ events because of the higher background rate. When a single top quark is produced, it is accompanied by only one other particle, a lighter quark or a W. In the t-channel technically the lighter quarks stay lighter quarks and are complicated to distinguish so that they do not contribute much in identifying a

single top quark event. Depending on the decay of the top quark, only a few jets (up to five but at least one) and a maximum of two charged leptons can be observed. Signals of this production mechanism of top quarks were first seen at the TEVATRON [21, 22].

2.2.3. Top Quark Decay

The decay of the top quark is determined by the CKM matrix, especially by the element V_{tb}. It gives the probability of the decay into a b-quark and a W^+-boson. Therefore the top decays almost always into a b-quark. Still, the other down-type quarks are possible with a really small fraction (~ 0.04 and ~ 0.001, see Section 2.1.2).

The produced b-quarks hadronize and form jets. A jet like this can be recognized as originating from the heaviest hadronizing quark quite easily because of the B mesons that can form in it. These can be identified amongst others if secondary vertices, where B mesons decayed, are found in a significant distance to the primary vertex.

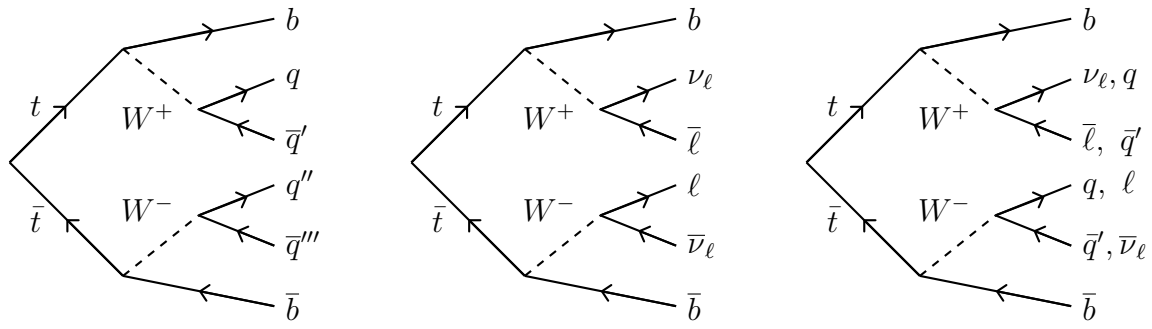

(a) All-jets channel. (b) Dileptonic Channel. (c) Semileptonic channel.

Figure 2.3.: Second half of Feynman diagrams for $t\bar{t}$ events, the production is left out.

The W-boson can decay either hadronically into a light quark and a light antiquark (u, d, s, c) with a probability of $(67.41 \pm 0.27)\,\% \approx \frac{2}{3}$ [16] or leptonically into a charged lepton (e, μ, τ) and its neutrino at a probability of $32\,\% \approx \frac{1}{3}$ (each charged lepton equally likely). The leptonical decay into a τ and its neutrino is left out here and also in analyses as they are not easily identified because of the occurrence of hadronically decaying τ leptons. This makes a branching fraction of $\mathcal{B}_{\text{lep}} = \frac{2}{9}$ for the decay into e or μ and a branching fraction of $\mathcal{B}_{\text{had}} = \frac{2}{3}$ for a hadronic decay. Altogether this makes three different possibilities for the decay of a $t\bar{t}$ pair, shown in Fig. 2.3.

If both W-bosons decay hadronically it is called the *all-jets decay channel*. The advantage of this decay channel is that, first, the branching fraction $\mathcal{B}_{\text{alljet}} = \frac{4}{9}$ is larger than for both other channels. Second, there is no neutrino produced that has to be reconstructed by taking missing transverse energy into account. The disadvantage is that six jets occur

that have a resolution less accurate than for example an electron or a muon. But even more problematic about this signal is that it only consists of jets. As its background has high contributions of QCD interactions it looks exactly like the signal.

The second case pictured is the *dileptonic decay channel*. Here, both W-bosons decay leptonically so that the only two observed jets are clearly visible b-jets. The remaining tracks are signals with even higher resolutions due to the large transverse momentum of the electrons or muons. The main problem with this decay channel is the large missing energy that is produced by two invisible neutrinos that cannot be separated that easily. Another smaller disadvantage is that this channel has the lowest branching fraction of $\mathcal{B}_{\text{dilep}} = \frac{4}{81}$ [28].

Lastly, a third decay channel that lies between the two aforementioned is possible. In the *semileptonic decay channel*, or also called $\ell + jets$ *channel*, one of the two W-bosons decays hadronically while the other decays leptonically. That makes a branching fraction of $\mathcal{B}_{\text{semilep}} = \frac{8}{27}$. Also, the quality of the signatures is between the ones of the two others. The signal of two jets is less clear than the one of another charged lepton but here only one neutrino contributes to the missing energy so that theoretically, if everything is measured perfectly, all particles can be reconstructed almost exactly the way they were (minus the QCD background from the jets). This channel is the only important one for this thesis because the KLFitter is used here for the reconstruction of those events.

3. The ATLAS Experiment

This bachelor thesis about neutrino reconstruction with KLFitter has been developed within the ATLAS Collaboration.

ATLAS is one of the main four detectors of the Large Hadron Collider at CERN[1] in Geneva. At the moment this collider is the largest particle collider in the world with an circumference of 26.7 km [29].

The following chapter presents the collider and the ATLAS experiment which is the important detector experiment for this thesis. The later used samples are simulated to be events at a centre-of-mass-energy of $\sqrt{s} = 8\,\text{TeV}$ which was the last setting of Run I. Therefore the experimental set-up of Run I is described. For Run II the Insertable B-Layer (IBL) was added to the tracking system of the detector [30].

The last section introduces the common coordinate system in dealing with CERN data and important observables used for the analysis.

3.1. The Large Hadron Collider

The Large Hadron Collider (LHC) is a two-ring-superconducting-hadron accelerator and collider which is located in the already existing tunnel of the Large Electron Positron Collider (LEP). In Run I, it was able to produce proton-proton collisions at centre-of-mass energies of $\sqrt{s} = 7\,\text{TeV}$ (2010, 2011 dataset) and $\sqrt{s} = 8\,\text{TeV}$ (2012 dataset). At the recently started Run II, the collider is able to collide protons at centre-of-mass energies of up to $\sqrt{s} = 14\,\text{TeV}$.

Because the LHC collides particles with particles, it includes two rings with counter-rotating beams instead of one beam pipe where particle and antiparticle that circle in opposite directions share the same phase space.

In these beam pipes, the particles are focused by superconducting magnets that are cooled down with superfluid Helium to a temperature below 2 K so that they produce fields above 8 T. Focussing the beam is realized mainly with quadrupole magnets while

[1] European Organization for Nuclear Research, abbreviation originating from: Conseil Européen pour la Recherche Nucléaire

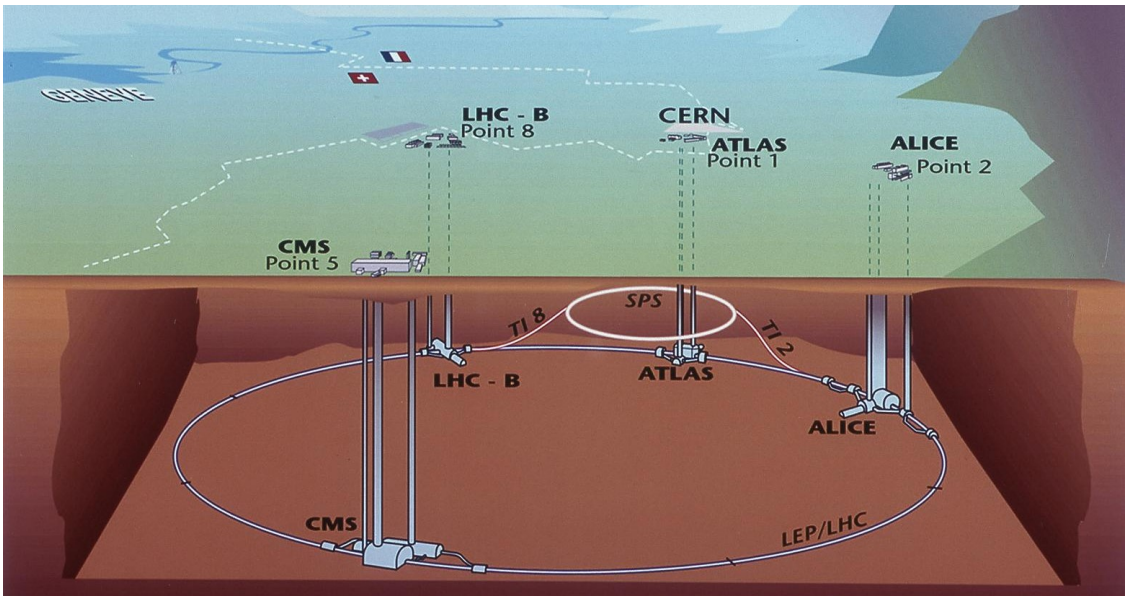

Figure 3.1.: The four main experiments at the LHC collider at CERN in Geneva.

for bending the particles trajectory to the needed circle dipole magnets are used.

Before the particle bunches are injected into the LHC tunnel they are accelerated to energies of 450 GeV by the CERN accelerator complex. Then the particle bunches are injected, accelerated by radio frequency cavities and stored inside the collider tunnel. This way, a total number of 2808 bunches each containing about 10^{11} protons can be stored inside the LHC [29].

There are four different interaction points with the four main detector experiments as shown in Fig. 3.1. The experiment named ALICE investigates collisions of heavy lead ions. It searches for hints of the possible existence of a quark-gluon plasma as well as looking at the behaviour of hadronic matter at high densities and temperatures [31]. LHCb uses an asymmetric detector covering only part of the phase space. Here physics at low scattering angles and examination of B mesons happens to observe CP-violation and discover physics beyond the Standard Model [32]. ATLAS and CMS are the largest detectors at the LHC and cover almost the complete solid angle around their collision point. At these experiments the Higgs boson is studied while also the search for dark matter candidates and hints of the theory of supersymmetry is ongoing [33, 34].

Besides the two main experiments, a few smaller ones exist near the interaction points. They search for example for magnetic monopoles (MoEDAL) [35] or elastic and diffractive cross sections (TOTEM) [36].

3.2. The Atlas Detector

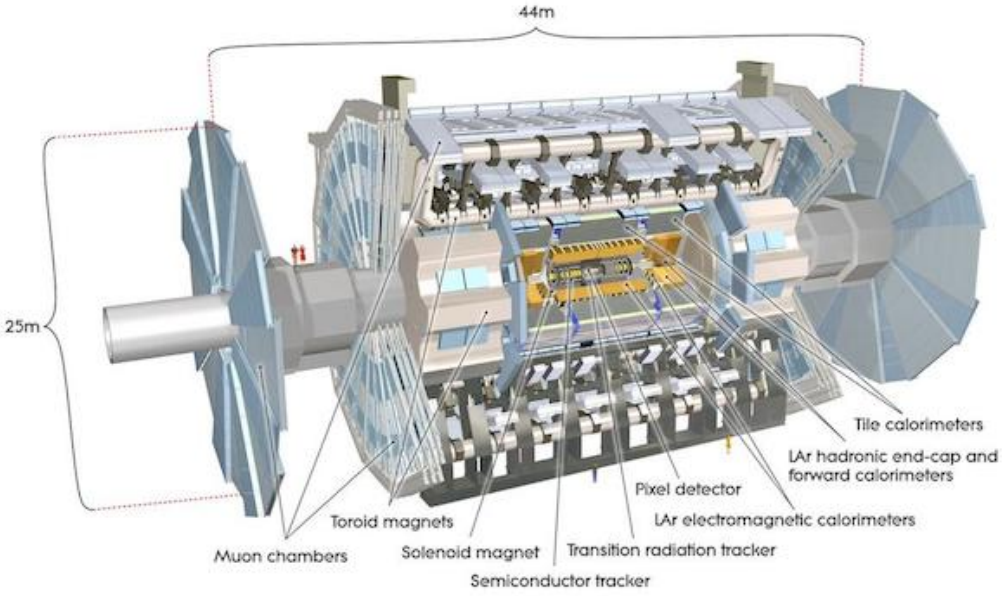

Figure 3.2.: Cut-away view of the Atlas detector and its subsystems [33].

Atlas (A Toroidal Lhc ApparatuS) is a detector which covers like Cms the complete solid angle and is able to measure particles up to a pseudorapidity of $|\eta| = 4.9$.

The whole detector system has a weight of approximately 7000 t, is about 44 m long and 25 m high. It consists of various layers of tracking chambers, calorimeters and muon chambers. Unlike detectors built for a specific purpose, Atlas can perform measurements for many different studies. Its structure is shown in Fig. 3.2.

In the inner detector the tracking chambers are located. These trace the trajectories of charged particles and are important for b-tagging. b-tagging means that b-quarks are likely to be the source of the observed jet. This can be seen amongst others if a secondary vertex has a significant distance to the primary vertex or interaction point.

Because of the high luminosity of the Lhc, a pile-up can happen where many of the about 30 different proton-proton collisions of a bunch crossing interfere in the detector [37]. An excellent tracking system as used in the Atlas detector is needed to separate and measure the single events.

This tracking system is realized in three different ways here. The biggest spatial resolution is delivered by the *Silicon Pixel Detector* with a minimum distance of $R \geq 4.55\,\text{cm}$ from the interaction point and 80 million read-out channels. Around the Pixel Detector there is the *Silicon Microstrip Tracker* consisting of small silicon strips instead of pixels.

The outermost tracking layer is formed by the *Transition Radiation Tracker*. It gives additional tracking information by measuring the transition radiation. This allows separating lighter particles (like electrons) from heavier particles (like pions). It has approximately 351,000 read-out channels. The whole tracking system gives a momentum resolution of $\sigma_{p_\mathrm{T}}/p_\mathrm{T} = 0.05\,\% \cdot p_\mathrm{T}[\mathrm{GeV}] \oplus 1\,\%$ [33].

Outside of the tracking system is the electromagnetic and hadronic calorimeter. Those need to specify the energies of electrons, photons and jets very precisely and also need a high spatial resolution. The measurement is done by producing particle showers inside the detector material. In the ATLAS detector the electromagnetic part is surrounded by the hadronic calorimeter so that in the inner part only the light particles are stopped completely with an energy resolution of $\sigma_E/E = 10\,\%/\sqrt{E[\mathrm{GeV}]} \oplus 0.7\,\%$. Except for muons and neutrinos all other particles are stopped by the hadronic layer. There the energy resolution is depending on the position but can be a maximum of $\sigma_E/E = 50\,\%/\sqrt{E[\mathrm{GeV}]} \oplus 3\,\%$. Both calorimeters are built as sampling calorimeters. The electromagnetic calorimeter consists of liquid Argon (LAr) as active material and lead as absorber while the hadronic one uses mostly stainless steel as absorber and scintillation plates as active material [33].

Muons do not emit enough Bremsstrahlung to be stopped by the calorimeters. This means for their detection muon chambers are needed. These form the outermost layer of the whole detector system at the ATLAS experiment. They have about a million read-out channels and deliver an absolute momentum resolution of $\sigma_{p_\mathrm{T}}/p_\mathrm{T} = 10\,\%$ at an energy of 1 TeV [33].

The different tracks inside of the ATLAS detector of all known particles are shown in Fig. 3.3. By seeing the specific track pattern the type of the originating particle can be determined.

3.3. Detector Coordinate System

In analyses of the data provided by the ATLAS detector, a right-handed coordinate system is used where the beam direction symbolizes the z-axis. The x-axis points from the interaction point in the centre of the detector to the centre of the large collider ring. The y-axis goes upwards. Based on this, the more important cylindrical coordinates (r, θ, ϕ) can be defined. The value r gives the radial distance from the z-axis (beam pipe) to the defined coordinates. The azimuthal angle ϕ lies in the x-y-plane. The polar angle θ is defined as the angle from the beam axis to the particle's flight direction. But instead of

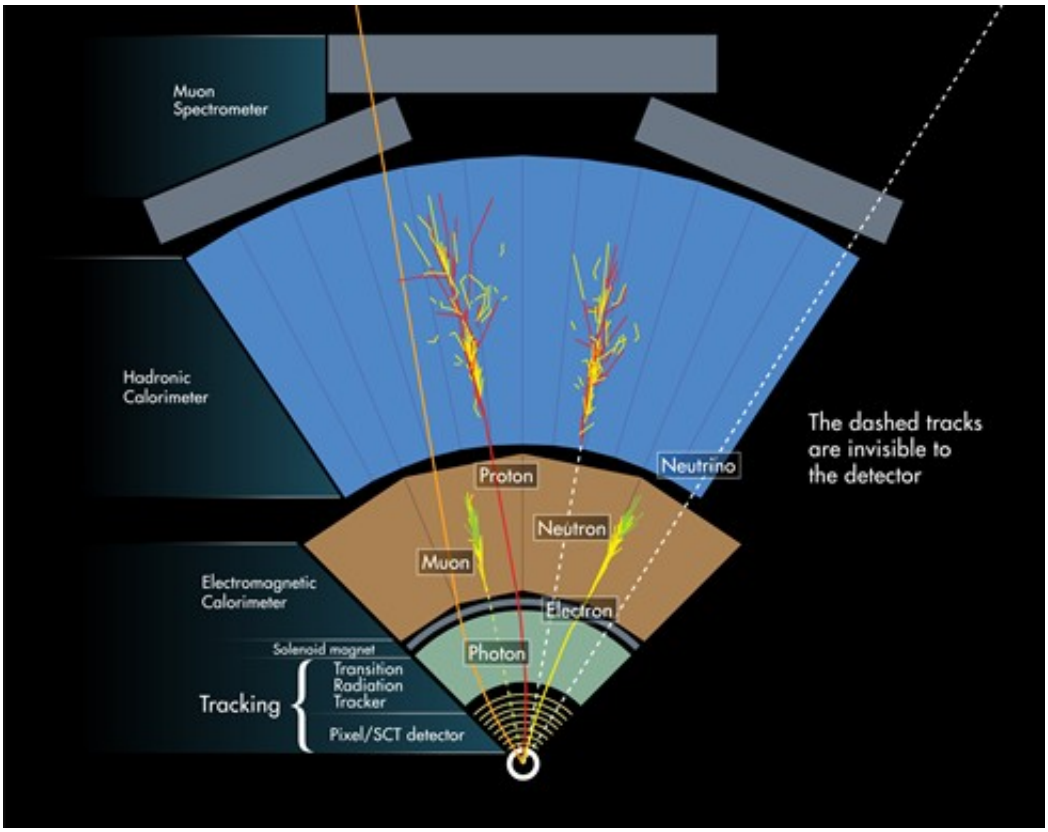

Figure 3.3.: Tracks, as they are visible in the ATLAS detector (©CERN).

the polar angle θ often the *pseudorapidity* may be more useful. It is defined as

$$\eta = -\ln\left(\tan\frac{\theta}{2}\right)$$

and differences in it are invariant under Lorentz boosts along the z-axis. Another useful parameter is the distance in the η-ϕ-plane defined as

$$\Delta R = \sqrt{\Delta\phi^2 + \Delta\eta^2}.$$

ΔR is one of the important variables in this analysis.

4. Kinematic Fitting

The KLFitter, which stands for *Kinematic Likelihood Fitter*, is a framework that reconstructs collision events with $t\bar{t}$ pairs in the ATLAS detector [38]. This C++ tool is based on the Bayesian Analysis Toolkit (*BAT*) [39].

As the goal of this thesis is to increase the reconstruction efficiency of KLFitter for the neutrino in the semileptonic decay channel of $t\bar{t}$ events, this chapter introduces the main programs used. First, the Monte Carlo data samples are explained which were used for the whole performance analysis. Next, the KLFitter framework itself is presented. It was the initial point in improving the matching efficiency. In this context, the underlying structures for the neutrino matching in particular are discussed.

When investigating reconstruction efficiencies, one needs parameters for quantification and a program that tests the output quality of the previous program. For this purpose, the MatchMonster framework is used. This C++ based framework is explained in the last section of this chapter.

4.1. Monte Carlo Data Sample

The here presented studies were performed on a certain Monte Carlo data sample saved as ROOT file. It contains only events with semileptonic and dileptonic final states of $t\bar{t}$ decay events. It was produced with the use of Powheg+Pythia, a next-to-leading-order Monte Carlo event generator [40, 41]. The data was generated to simulate events at a centre-of-mass energy of $\sqrt{s} = 8\,\text{TeV}$ and at a top pole mass of $172.5\,\text{GeV}$.

After generation, the events were passed to the ATLAS simulation software and reconstructed by using the ATHENA framework [42]. It contains a total number of about $3,047,000$ events in the electron and about $3,595,000$ events in the separate muon sample. The b-tag information was added to the data sample by the MV1-tagger operating at a working point with $70\,\%$ efficiency.

For the creation of the sample that only contains semileptonic events, the following object definitions were used:

- Only electrons with $p_\text{T} > 25\,\text{GeV}$ and $|\eta| < 2.47$ excluding the crack-region (see

below) are passed.

- Only muons with $p_{\mathrm{T}} > 25\,\mathrm{GeV}$ and $|\eta| < 2.5$ are passed.
- Jets which are reconstructed by an anti-k_t algorithm [43] with a size which equals the radius in the η-ϕ-plane of 0.4, need to have $p_{\mathrm{T}} > 25\,\mathrm{GeV}$ and $|\eta| < 2.5$.
- Events need to have $E_{\mathrm{T}}^{\mathrm{miss}} > 20\,\mathrm{GeV}$ and fulfil the triangular cut $E_{\mathrm{T}}^{\mathrm{miss}} + m_{\mathrm{T}W} > 60\,\mathrm{GeV}$.

The so-called "crack region" ($1.37 < |\eta| < 1.52$) is the region between the barrel and forward calorimeters in a detector. Electrons that are detected here cannot be reconstructed reliably and are therefore excluded from analyses.

Furthermore, jets that are overlapping with the tracks of charged leptons are removed if their distance is $\Delta R < 0.2$. This is important because the jet algorithm reconstructs most electrons as jets.

4.2. The KLFitter Framework

The KLFitter framework has a modular structure so that even though it was developed for the reconstruction of $t\bar{t}$ events at the ATLAS detector at $\sqrt{s} = 7\,\mathrm{TeV}$, by changes KLFitter can be adjusted to a new detector or different centre-of-mass energies. It gives four-vectors that can be saved to a ROOT file by MiniKLFitter, which is an interface for KLFitter [38].

The correct reconstruction of the considered events is important for precision measurements for example for measuring the mass of the top quark. If the jets of the decay are not assigned correctly here, the study is not as good. The method of kinematic likelihood fitting was found to be the best up to now as it is based on the most accurate description of the underlying physics processes and takes detector effects into account.

Before the KLFitter is fed with data, they first have to pass the event selection. This is not relevant for the used set-up of KLFitter as the used samples already passed an even stronger event selection.

Next the four jets to be used for the reconstruction are chosen. Amongst them are all b-tagged jets. The remaining slots are filled by the non b-tagged with the highest p_{T} values.

There is only one charged lepton that can be matched to the lepton's signal unmistakably. So, the four chosen jets are remaining to be matched to the underlying decay jets. This makes 24 possible permutations. Because the two jets from the hadronically

decaying W are not relevant to be distinguished to fit the masses of the W and its mother particle, the top quark, a possible setting of KLFitter now leaves twelve permutations left to be analysed. In case of two (one) b-tags there are only two (six) permutations left. The used setting here provides weights for the likelihoods according to the b-tag probabilities.

For every permutation of an event, its likelihood is calculated. This gives a value for measuring the probability that the event is observed with the considered parameters and is defined as [38]

$$\begin{aligned} L = & B(m_{q_1q_2b_{\mathrm{had}}}|m_{\mathrm{top}},\Gamma_{\mathrm{top}}) \cdot B(m_{q_1q_2}|m_W,\Gamma_W) \\ & \times B(m_{\ell\nu b_{\mathrm{lep}}}|m_{\mathrm{top}},\Gamma_{\mathrm{top}}) \cdot B(m_{\ell\nu}|m_W,\Gamma_W) \\ & \times \prod_{i=1}^{4} W_{\mathrm{jet}}(E_{\mathrm{jet},i}^{\mathrm{meas}}|E_{\mathrm{jet},i}) \cdot W_\ell(E_\ell^{\mathrm{meas}}|E_\ell) \\ & \times W_{\mathrm{miss}}(E_x^{\mathrm{miss}}|p_x^\nu) \cdot W_{\mathrm{miss}}(E_y^{\mathrm{miss}}|p_y^\nu). \end{aligned}$$

The formula contains different elements about the detector and the quality of the measurement:

- $B(m_{q_1q_2b_{\mathrm{had}}}|m_{\mathrm{top}},\Gamma_{\mathrm{top}})$: Breit-Wigner function as probability distribution of the expected mass of the top quark in consideration of the true mass and decay width. The probability is dependent on the invariant mass of two light quarks (and therefore the W) and the correct one of the b-quarks.

- $B(m_{q_1q_2}|m_W,\Gamma_W)$: Breit-Wigner function as probability distribution of the expected mass of the W in consideration of the true mass and decay width. The probability is dependent on the invariant mass of the two reconstructed light quarks.

- $B(m_{\ell\nu b_{\mathrm{lep}}}|m_{\mathrm{top}},\Gamma_{\mathrm{top}})$: Breit-Wigner function as probability distribution of the expected mass of the top quark in consideration of the true mass and decay width. The probability is dependent on the invariant mass of the charged lepton and neutrino (and therefore the W) and the correct one of the b-quarks.

- $B(m_{\ell\nu}|m_W,\Gamma_W)$: Breit-Wigner function as probability distribution of the expected mass of the W in consideration of the true mass and decay width. The probability is dependent on the invariant mass of the charged lepton and the neutrino.

- $W_{\mathrm{jet}}(E_{\mathrm{jet},i}^{\mathrm{meas}}|E_{\mathrm{jet},i})$: Transfer function for the energy resolution of one of the four jets. It appears once for each jet in the likelihood but is different for light jets and b-jets.

- $W_\ell(E_\ell^{\mathrm{meas}}|E_\ell)$: Transfer function for the energy resolution of the charged lepton.

- $W_{\text{miss}}(E_x^{\text{miss}}|p_x^\nu)$: Transfer function for the momentum of the neutrino in dependency on the resolution of $E_{\text{T}}^{\text{miss}}$ in x-direction.
- $W_{\text{miss}}(E_y^{\text{miss}}|p_y^\nu)$: Transfer function for the momentum of the neutrino in dependency on the resolution of $E_{\text{T}}^{\text{miss}}$ in y-direction.

The probability distributions that are called $B(x|y,z)$ are Breit-Wigner functions where y is the location parameter where the peak of the function is and z is the scale parameter which specifies the width of the distribution. x, then, is the function's parameter where the corresponding probability is to be known. For the transfer functions approximated with $W(x|y)$ Gaussian shapes were chosen. Except for the ones for the missing transverse energy in x and y directions which are each a single Gaussian function, all transfer functions are implemented as double Gaussian functions.

Instead of maximizing the weighted likelihood, the value of $-\ln L$ is minimized. The reason for this is that the available software libraries provide minimizations rather than maximizations. Another reason is that the logarithm of the likelihood is preferred over the likelihood itself because adding logarithms is numerically more stable than multiplying values. Also multiplying the likelihood parts takes much more computation time than adding logarithms of them.

For minimization, KLFitter smears the energies and momenta in agreement with the detector resolutions (taking a value that is less probable will make the total event's likelihood worse) until the Likelihood is at a maximum value. The permutation with the highest value of the weighted likelihood (the smallest weighted $-\ln L$) is defined as the best. This still does not imply which permutation is the true one.

These running options were successfully used in a large number of analyses (e.g. [44–46]). But also other running options are possible. For example, the fitter can be adjusted to any arbitrary process and final state simply by writing a new likelihood for it.

4.2.1. Neutrino Reconstruction

For this thesis, an accurate knowledge of how the KLFitter operates when reconstructing the neutrino is necessary. Thus, the procedure is discussed in detail in this section.

Before reconstructing anything, boundaries of different entries of the momentum vector, p_x^ν as well as p_y^ν and p_z^ν have to stay in the range of $-1000\,\text{GeV} < p_i < 1000\,\text{GeV}$.

Next p_x^ν and p_y^ν are set to be in the range of $E_{x,y}^{\text{miss}} - \sigma < p_{x,y}^\nu < E_{x,y}^{\text{miss}} + \sigma$ where σ is calculated by taking the transfer functions into account. As a starting value for the momentum for the following fits the measured missing energy is used, which means $p_x^\nu = E_x^{\text{miss}}, p_y^\nu = E_y^{\text{miss}}$.

Now the neutrino p_z^ν is calculated. This is done via the invariant mass of the leptonically decaying W-boson. Here, the four-momenta are essential for

$$m_W^2 = \left(p^\nu + p^\ell\right)^2 .$$

With $E^2 = m^2 + p^2$ and $m_\nu \approx 0$ it gives the quadratic equation

$$a \cdot (p_z^\nu)^2 + b \cdot p_z^\nu + c = 0, \tag{4.1}$$

with

$$\begin{aligned} a &= (p_z^\ell)^2 - (E^\ell)^2 \\ b &= \alpha \cdot p_z^\ell \\ c &= \frac{\alpha}{4} + E^\ell \cdot \left[(p_x^\nu)^2 + (p_y^\nu)^2\right] \\ \alpha &= m_W^2 - m_\ell^2 + 2\left(p_x^\nu p_x^\ell + p_y^\nu p_y^\ell\right). \end{aligned}$$

The mass of the W-boson is well known by previous experiments and therefore set as constant. Also constant are p_x^ν and p_y^ν that are the measured missing energy vector entries. So this equation is solved by

$$p_z^\nu = \frac{-b \pm \sqrt{b^2 - 4ac}}{2a} \tag{4.2}$$

and has either zero or two solutions depending on the value of the discriminant. The case of exactly one solution has not been observed during the analyses for this thesis even though it may be possible.

If the equation has no solution, KLFitter has to choose any starting value of p_z^ν. As the distribution of the true neutrino p_z has a peak at $p_z = 0$, the default choice is $p_z^\nu = 0$.

If the equation has two solutions, both solutions are written into the p_z solution vector. Then the likelihood of both these possible starting p_z^ν values is calculated and the one with the higher value is chosen for the following fit.

So up to here everything is prepared to start the actual kinematic fitting. For getting the highest possible likelihood of the single event besides all jet energies and so on, also the p_x^ν and p_y^ν values are smeared according to the transfer functions of $E_{\mathrm{T}}^{\mathrm{miss}}$. As no transfer function exists for the p_z^ν, it is varied in a way so that the mass of the W-boson stays constant under smearing of p_x^ν and p_y^ν.

As reconstructed quantities, the ending value of p_z^ν of the fit as well as the starting values of p_x^ν and p_y^ν from the best permutation (the permutation with the highest weighted

likelihood) are output.

4.3. The MatchMonster Framework

For finding the quality of the KLFitter output a small C++ program called MatchMonster is used. Besides copying all relevant input ROOT trees into the output files it also adds new branches. The matching criterion is that the true particle vector from the Monte Carlo simulations and the reconstructed particle vector have a distance ΔR in the η-ϕ-plane that is is smaller than 0.3. In this way the matching of all particles of an event is checked and the corresponding parameter is set to either 0 or 1. For example, if the distance of the reconstructed and true neutrino is $\Delta R = 0.23$ the vectors match and the parameter *numatched* is 1.

Besides adding branches, the MatchMonster also generates histograms that show selected matching efficiencies depending on different cuts on the data.

For example the histogram that the reconstruction efficiencies in this thesis are taken from only takes events into account that fulfil the variables *isLjets = 1*, *multimatch = 0* and *alljetswithinfour* = 1. This means that the event must contain the signal of a charged lepton, no reconstructed particle that is assigned to more than one decay particle and all chosen jets for the reconstruction must be the four highest momentum jets.

5. Results and Discussion

In this chapter, the studies about the neutrino reconstruction in the KLFitter framework as well as their results are presented.

The first section explains how performing different cuts on the data can improve the reconstruction efficiency of the neutrino while the second section draws connections to the matching of other particles.

After that, the MatchMonster framework is analysed. This is to make sure it depicts the true quality of the KLFitter output and compares the appropriate values. Lastly, the KLFitter itself gets tested and improved to perform in the best possible way.

The *reconstruction efficiency* mentioned above is defined as the fraction of the data sample that fulfils the criterion of $\Delta R < 0.3$ for the regarded particle. This means that the distance of the true particle from the Monte Carlo simulation and the particle that was reconstructed by KLFitter is very small in the η-ϕ-plane.

Because KLFitter should always be able to reconstruct a certain event, it is necessary for the particular event to fulfil the criteria mentioned in Section 4.3. Only in that case it may be reconstructed and is included in the statistics.

The following results were produced for samples for the $e+$jets and $\mu+$jets channels. In this chapter, only the results for the muon samples are shown because it contains slightly more events. All plots and tables for the electron sample can be found in the appendix in Appendix A while the corresponding tables can be found in Appendix B.

Matching	Efficiency [%]
Muon	98.85
Leptonic b	84.21
Hadronic b	76.97
All partons	39.56
Hadronic t	74.50
Leptonic t	44.87
Neutrino ν	21.57

Table 5.1.: Reconstruction efficiencies of important decay particles in the $\mu+$jets channel before the analysis as shown in Fig. 5.1(a).

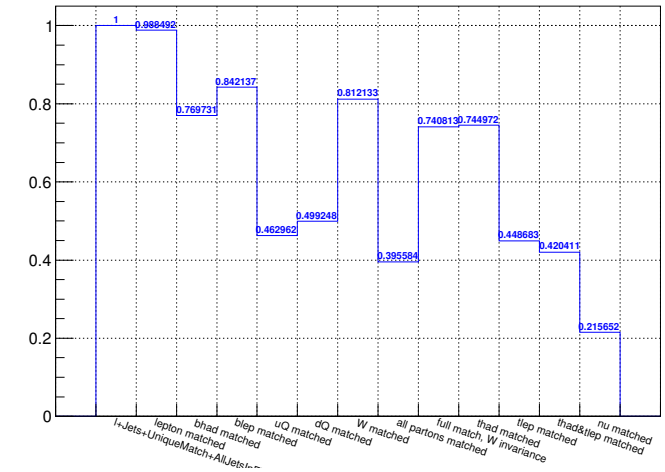

(a) Reconstruction efficiencies.

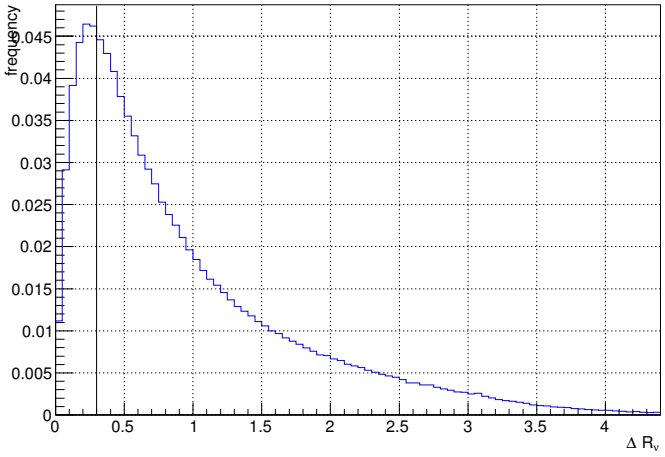

(b) ΔR distribution for the neutrino.

Figure 5.1.: Status of the reconstruction efficiency before the analysis. At the top are the efficiencies of all regarded particles and at the bottom is the distribution of ΔR for the neutrino.

In Fig. 5.1, the initial reconstruction efficiencies before applying modifications is shown. The exact values depicted here are also summarized in Table 5.1. Those plots and tables illustrate the initial settings characterizing the starting point.

5.1. Possible Cuts for Data Analysis

Before looking into the important programs the output files themselves and the correlations between the neutrino reconstruction and different measured values are crucial.

As shown in Fig. 5.2(a),(c),(e) the quality of the neutrino reconstruction is heavily dependent on the number of b-tags as well as the values of $E_{\mathrm{T}}^{\mathrm{miss}}$ and $m_{t\bar{t}}$. To explain the chosen ranges for the plot, the distributions of the three parameters over all events are shown in Fig. 5.2(b),(d),(f).

Thus, if a high neutrino reconstruction efficiency is desired for a special analysis, it is recommended to cut the data on one of these values. For this, the individual improvements and the loss on statistics are listed in Table 5.2.

Cut Parameter	Improvement [%]	Remaining Statistics [%]
At least one b-tag	-0.06	93.56
At least two b-tags	0.46	61.27
At least three b-tags	0.80	6.21
Four b-tags	5.72	0.04
$E_T^{\mathrm{miss}} > 50,000\,\mathrm{GeV}$	6.65	76.32
$E_T^{\mathrm{miss}} > 100,000\,\mathrm{GeV}$	24.28	20.06
$E_T^{\mathrm{miss}} > 150,000\,\mathrm{GeV}$	37.96	5.08
$E_T^{\mathrm{miss}} > 200,000\,\mathrm{GeV}$	44.37	1.43
$m_{t\bar{t}} > 400\,\mathrm{GeV}/c^2$	1.79	94.92
$m_{t\bar{t}} > 500\,\mathrm{GeV}/c^2$	6.77	51.85
$m_{t\bar{t}} > 600\,\mathrm{GeV}/c^2$	11.09	26.77

Table 5.2.: Improvement of the neutrino reconstruction efficiency and remaining statistics when performing special cuts on the used data. The improvement gives the value that needs to be added to the efficiency of the whole sample. The remaining statistics gives the percentage of the sample that is left for analysis after performing the cut.

5.2. Dependency of Neutrino Reconstruction Efficiency on Matched Particles

The reconstruction of the neutrino is closely linked to the reconstruction of other decay particles. This is because its momentum is calculated via the invariant mass of the W-boson which is connected to the invariant mass of the leptonically decaying top quark as described in Section 4.2.1.

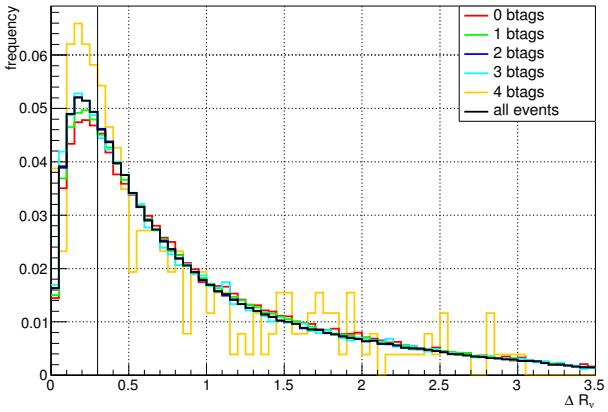

(a) b-Tags cut.

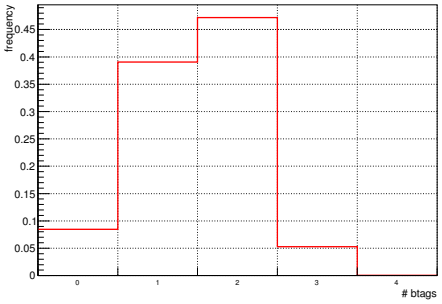

(b) b-Tags distribution.

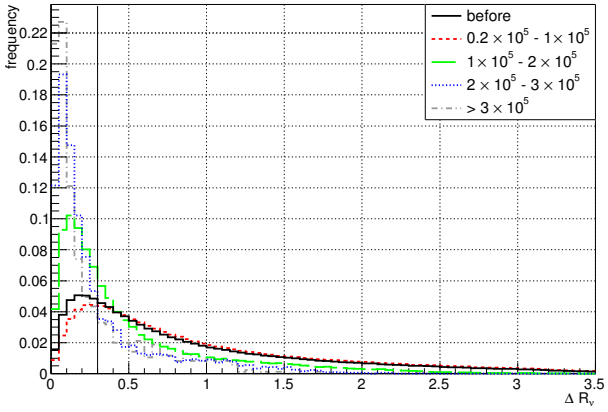

(c) $E_{\mathrm{T}}^{\mathrm{miss}}$ cut.

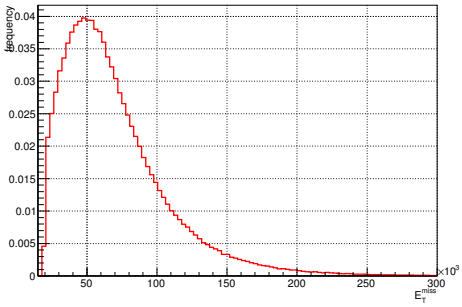

(d) $E_{\mathrm{T}}^{\mathrm{miss}}$ distribution.

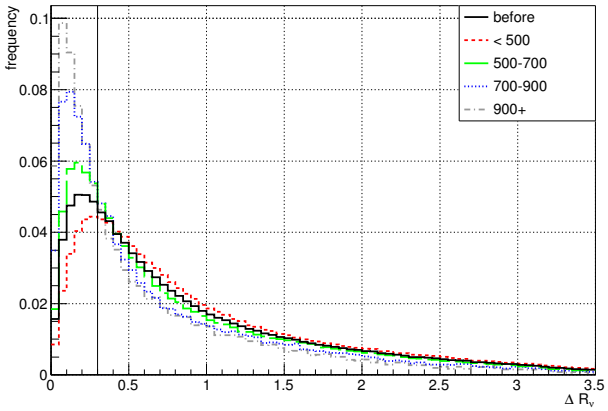

(e) $m_{t\bar{t}}$ cut.

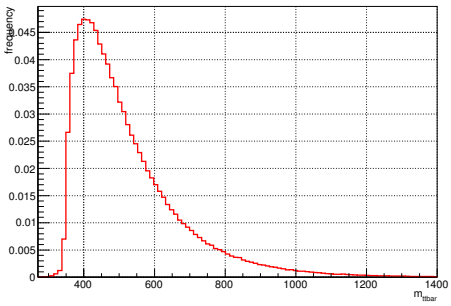

(f) $m_{t\bar{t}}$ distribution.

Figure 5.2.: On the right side are the distributions of the possible cut parameters in the analysed sample. On the left side is the ΔR distribution for various ranges of possible cut parameters in analyses. The fraction of events that are below $\Delta R = 0.3$ increases with the number of b-tags, higher $E_{\mathrm{T}}^{\mathrm{miss}}$ and higher $m_{t\bar{t}}$. For these plots, the output files after all improvements in the codes were used.

If, for example, the leptonic b-quark is reconstructed correctly ($\Delta R_{b_{\text{lep}}} < 0.3$) it is more likely that also the neutrino is reconstructed correctly as shown in Fig. 5.3.

These dependencies are not accessible in real data and do not represent any value to cut on data. Still, they demonstrate the procedure and consistency of the fit mechanism very well.

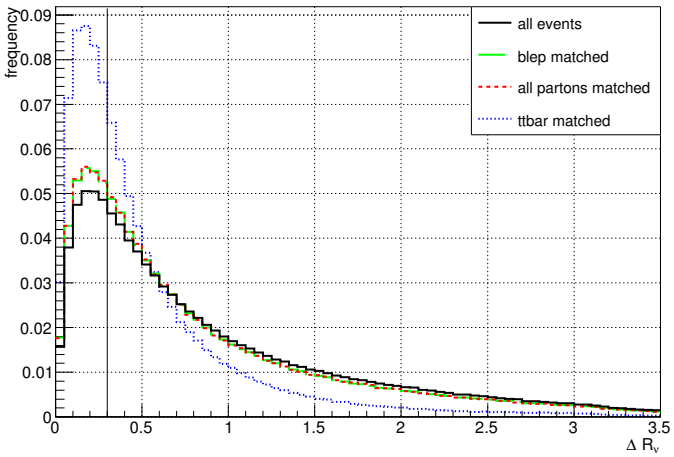

Figure 5.3.: Distribution of ΔR for the neutrino for a correctly reconstructed leptonic b-quark, all partons and the whole $t\bar{t}$ system. The first is fulfilled by about 84.35 %, the second by about 39.63 % and the latter by about 46.01 %. The first increases the reconstruction efficiency for the neutrino by about 3.05 %, the second by about 3.12 % and the latter by about 18.74 %. For this plot, the output files after all improvements in the codes were used.

5.3. General Improvements in Code

To find reasons for the high values of ΔR for the neutrino, the parameters of its calculation are examined. As $\Delta R = \sqrt{(\Delta\eta)^2 + (\Delta\phi)^2}$, η and ϕ should be investigated. Here, the focus lies on studying the momentum p of the neutrino. It is highly correlated with η and ϕ but its components p_x, p_y and p_z can be accessed separately in KLFitter and its output files. This is done in Fig. 5.4. Analogous plots for $\Delta\eta$ and $\Delta\phi$ can also be found in the appendix in Fig. A.4 and may be subject to further research.

While Δp_x and Δp_y look satisfying as they even have a smaller width than the equivalent jet distributions, Δp_z behaves unusual. The neutrino distribution is much worse than the jet distribution which applies to all values. For a closer look in Fig. 5.5, p_z^{reco} is plotted against p_z^{true}. This illustrates as well that the reconstructed value has a comparatively

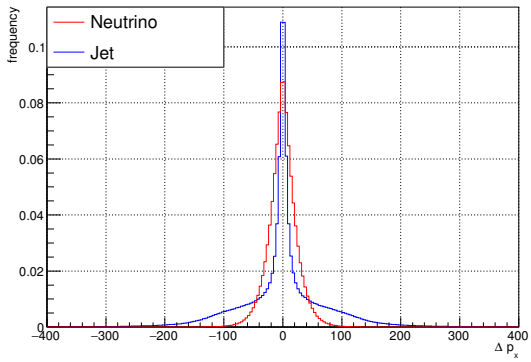

(a) Δp_x.

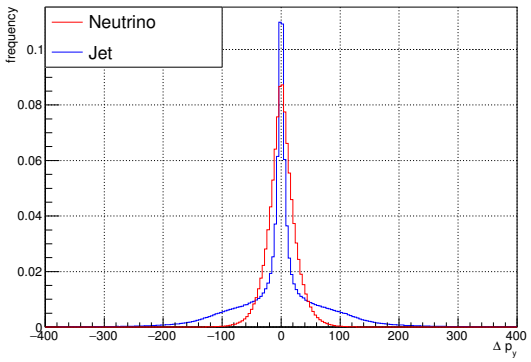

(b) Δp_y.

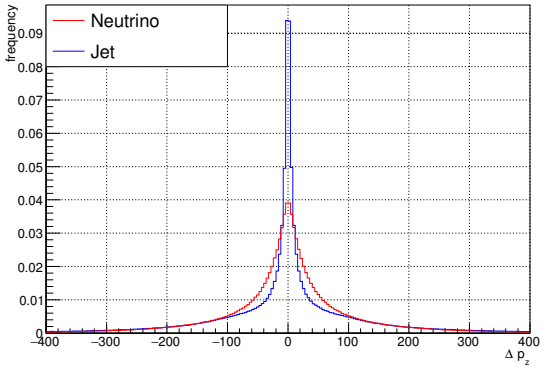

(c) Δp_z.

Figure 5.4.: Difference between true and reconstructed entries of the momentum vector compared for the neutrino and a jet. As jet the hadronic b-jet is chosen since it has less decay correlation with the neutrino than the leptonic b but a better reconstruction efficiency than the light quarks.

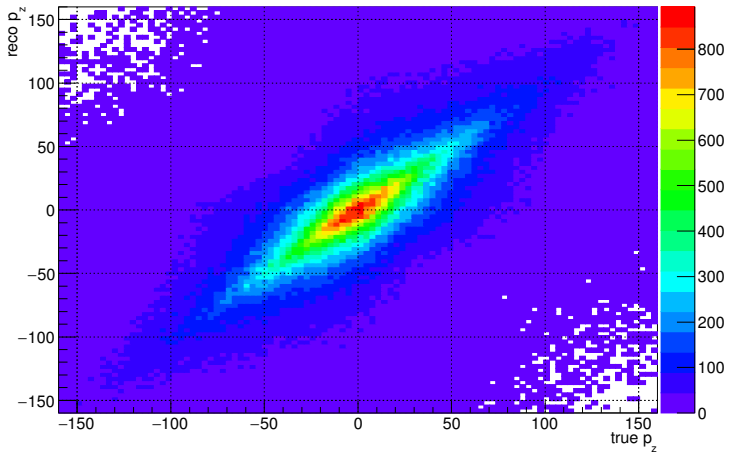

Figure 5.5.: Distribution of p_z^{reco} to p_z^{true} for the neutrino in the analysed data.

large deviation from the true value. Based on this, the following approaches for improving the KLFitter performance are implemented and tested.

5.3.1. Improvements in MatchMonster

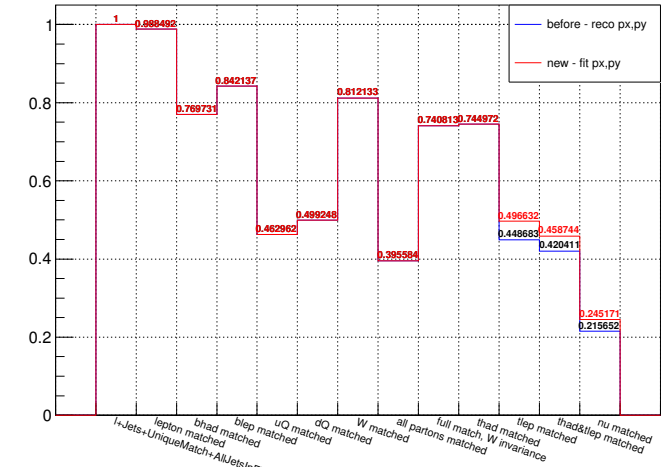

(a) Reconstruction efficiencies.

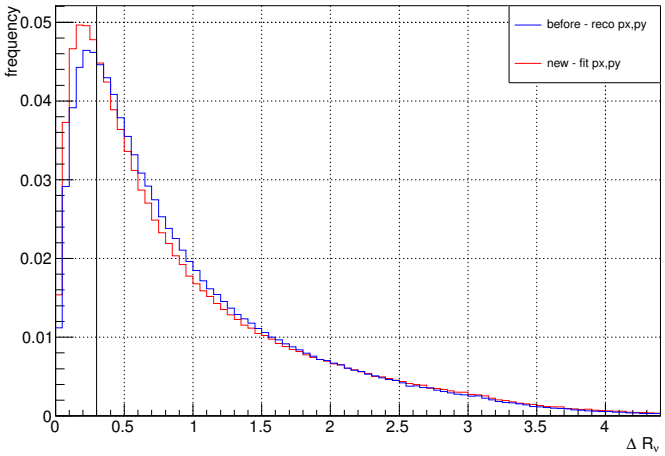

(b) ΔR distribution for the neutrino.

Figure 5.6.: Status of the reconstruction efficiency after improving the MatchMonster framework. At the top are the efficiencies of all regarded particles and at the bottom is the distribution of ΔR for the neutrino

p_x and p_y of the neutrino can be reconstructed based on the measured values of E_x^{miss} and E_y^{miss} before the fit is performed. This is not valid for the p_z as no momentum or energy value in the direction of the beam pipe can be measured. Therefore the reconstructed

value for p_z as called in the output file is equal to the fitted value for p_z while the fitted p_x and p_y are different from the reconstructed ones.

This may be contradictory to the momentum conservation when taking the vector (reco p_x, reco p_y, fitted p_z) for further calculations (reco = reconstructed). As MatchMonster takes exactly these values for comparing the reconstructed particles to the true ones it may not match as well as with vectors that conserve the momentum.

After changing the MatchMonster code so that now for the neutrino the fitted values are used for the comparison the neutrino reconstruction efficiency indeed could be raised by 2.95 %. With this also the efficiency values for the leptonic t-quark and the whole $t\bar{t}$ system increased as shown in Fig. 5.6.

5.3.2. Improvements in KLFitter

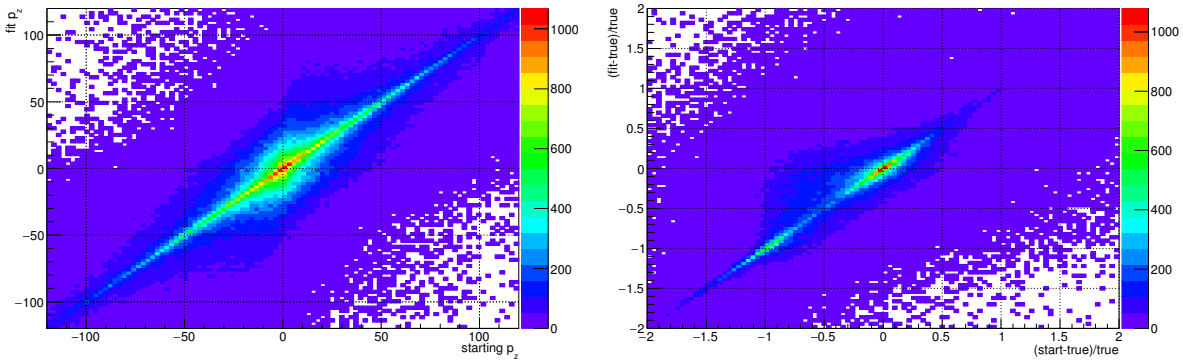

(a) Fitted p_z vs. starting p_z.

(b) Deviation of fitted p_z vs. deviation of starting p_z scaled to units of the true value.

Figure 5.7.: Studies on the dependencies of the fitted neutrino p_z value on the starting value of the fit. The fitted value is highly dependent on the value the fit starts with.

To understand what may go wrong with the neutrino inside of KLFitter, studying the connection between the starting value of the fit and the fitted value of p_z is necessary. This is shown in Fig. 5.7(a). In addition, the deviation of the fit value from the true value is plotted against the one of the starting value in Fig. 5.7(b). It can be seen that the fitted and the starting value are highly correlated as well as their deviations. This leads to the conclusion that a reasonable choice of the starting value is inevitable to get a good reconstruction efficiency.

As mentioned in Section 4.2.1 there are two possibilities for the quadratic equation (4.1) that gives the initial value of the fit. Either it has zero or two solutions. In dependency on

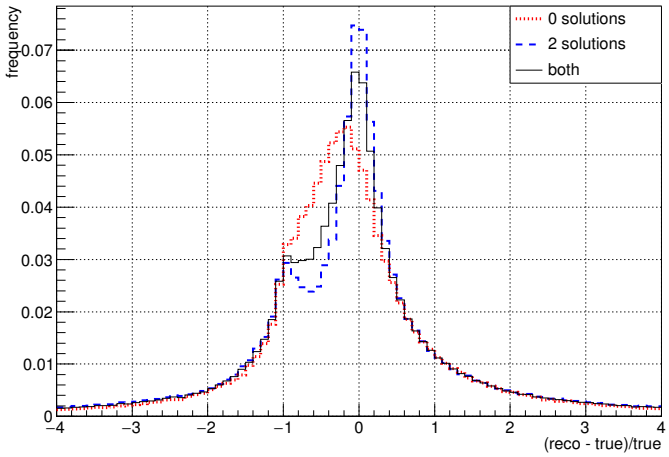

Figure 5.8.: Distribution of Δp_z scaled to p_z^{true} and plotted against the p_z^{true} value of the neutrino.

this, the reconstruction efficiency in both cases is useful. For that, the Δp_z distribution scaled to the true p_z is plotted separately for zero and two solutions in Fig. 5.8. It is clearly visible that in case of no solution the reconstruction is worse than in the two solution case. As the value on the x-axis is $\Delta_{\text{rel}} p_z = \frac{p_z^{\text{reco}} - p_z^{\text{true}}}{p_z^{\text{true}}}$, it is clear that the true value is very often higher than the one KLFitter reconstructs in the case of no solutions.

In this case, KLFitter sets the starting value for p_z in the fit arbitrarily to zero. Even though zero is the most probable value in the true distribution, it does not justify this choice for a single event.

Taking only the real part of the complex solution of Eq. (4.2) $p_z = \frac{-b}{2a}$ may be a better estimate. After implementing this in the KLFitter framework and looking into the usual plots showing the reconstruction efficiencies, no visible changes can be seen. So in Fig. 5.9, only the difference of the new implementation minus the status before is depicted. In the ΔR distribution in Fig. 5.9(b) as well as in the efficiency plot Fig. 5.9(a) can be seen that the new starting value in the zero solution case involves improvements not only for the neutrino, but also for all other decay particles except the charged lepton. The enhancement of 0.10 % for the neutrino is just slight but it suffices to justify the small change in the code.

For the sake of completeness it was tested whether KLFitter chooses the right one if two solutions exist. As shown in Fig. 5.10, when forcing the framework to choose the not preferred solution the reconstruction efficiency of the neutrino drops by about 5 % while also all other particles are affected. As the result was very clear also when taking the error bars in Fig. 5.10(b) into account, this test was not repeated on the large sample. Here it

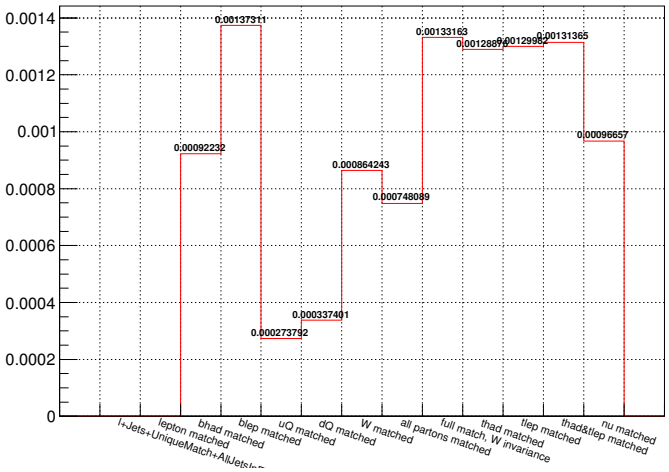

(a) Difference in the reconstruction efficiencies.

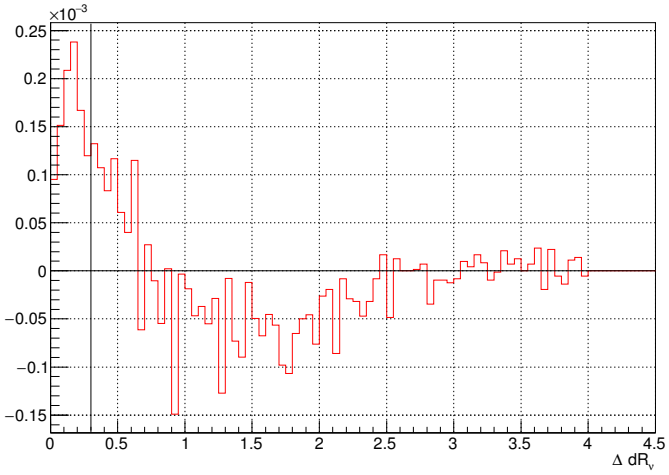

(b) Difference in the ΔR distribution for the neutrino.

Figure 5.9.: Differences in reconstruction efficiencies between the improved KLFitter framework after implementing the new zero-solution starting value and the status before.

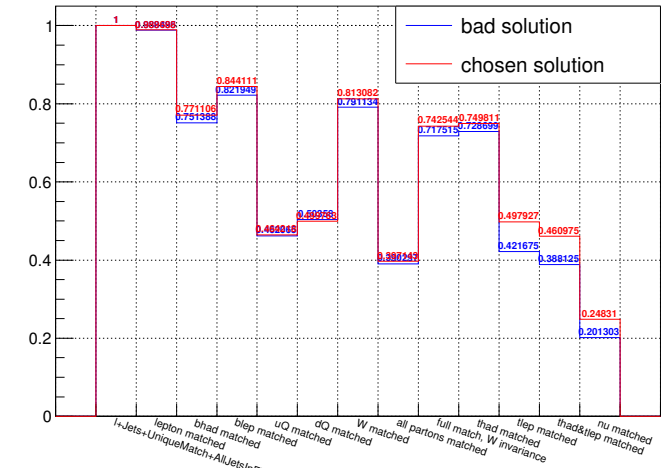

(a) Reconstruction efficiencies.

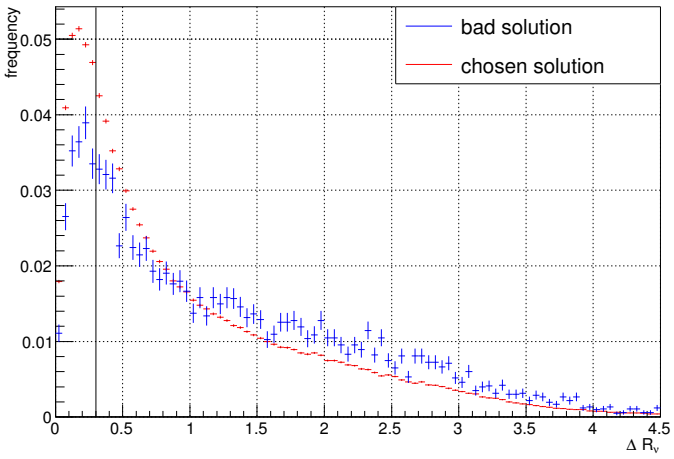

(b) ΔR distribution for the neutrino.

Figure 5.10.: Status of the reconstruction efficiency after forcing KLFitter to choose the bad solution in the two solution case.

was done using a small part of the sample of about 30,000 events that only contain the $e+$jets channel.

Now, that the starting value was adjusted, the fit mechanism needs to be inspected. For this, Fig. 5.11 shows the difference between p_z^{reco} and p_z^{true} against p_z^{reco}, one plot each for zero and two solutions. It can be seen there that the deviations of p_z^{reco} are immense, especially for very high and very low values of p_z^{true}.

The idea to fix this is to add another transfer function to the likelihood along the lines of the transfer functions for E_{jet} and E_ℓ. Geared to the distribution of p_z^{true} in Fig. 5.12, the sum of two Gaussian functions $p_z = \text{Gauss1} + \text{Gauss2}$ is chosen. Both mean values

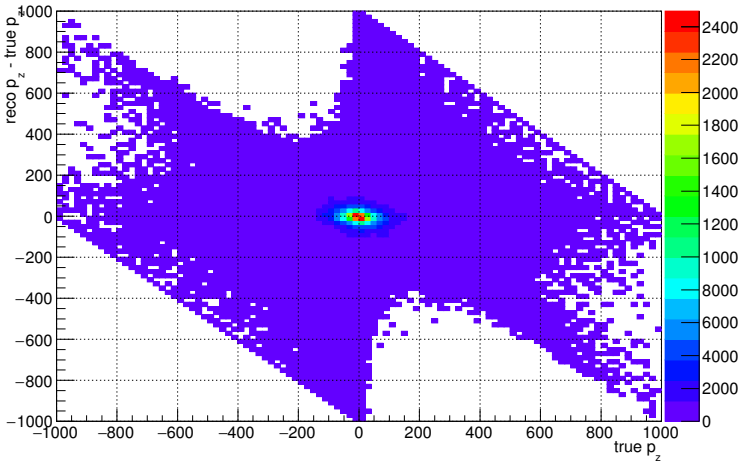

Figure 5.11.: The spreading of the difference between p_z^{reco} and p_z^{true} in dependency on p_z^{true} of the neutrino.

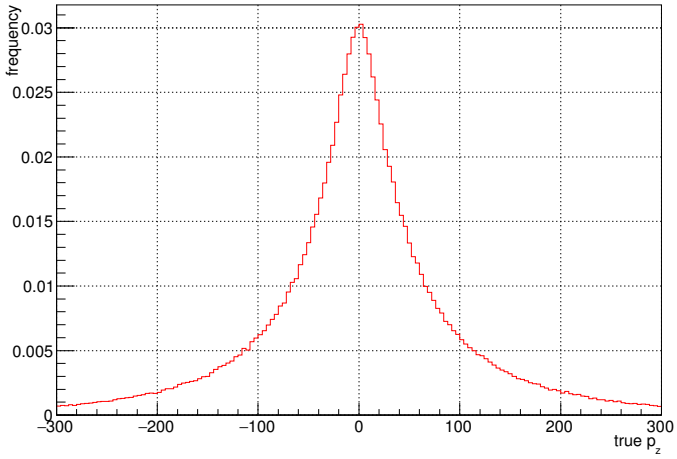

Figure 5.12.: Distribution of p_z^{true} of the neutrino in the used Monte Carlo samples for the $\mu+$jets channel.

are set to zero. As the neutrino is dependent on various parameters (see Section 5.1) the variables of the Gaussian functions used for the fit are made to be dependent on $E_{\text{T}}^{\text{miss}}$. The missing transverse energy was chosen first because it is directly connected to the neutrino. Second, all other cut parameters from Section 5.1 have disadvantages. The number of b-tags may vary depending on the used b-tagger and has much larger statistical uncertainties than the resolution of the detector. Also, it only delivers discrete numbers. This would make a total of five different transfer functions which may not be as precise as adjusting the transfer function continuously. The mass of the $t\bar{t}$ system drops out as well because it is a reconstructed quantity and depends on the likelihood itself. Fig. 5.13 shows

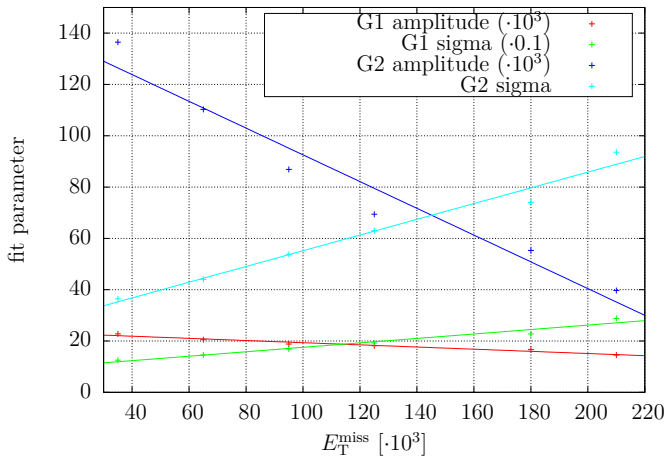

Figure 5.13.: Linear Fits for the parameters of the Double Gaussian distribution for the transfer function in dependency on $E_{\mathrm{T}}^{\mathrm{miss}}$.

the linear dependencies of the different fit parameters for the double Gaussian function on $E_{\mathrm{T}}^{\mathrm{miss}}$. For considering these dependencies in the implementation, the linear functions are taken as fit variables for the double Gaussian distribution in the transfer function.

The final updated likelihood is now

$$\begin{aligned} L = & B(m_{q_1q_2b_{\mathrm{had}}}|m_{\mathrm{top}},\Gamma_{\mathrm{top}}) \cdot B(m_{q_1q_2}|m_W,\Gamma_W) \\ & \times B(m_{\ell\nu b_{\mathrm{lep}}}|m_{\mathrm{top}},\Gamma_{\mathrm{top}}) \cdot B(m_{\ell\nu}|m_W,\Gamma_W) \\ & \times \prod_{i=1}^{4} W_{\mathrm{jet}}(E_{\mathrm{jet},i}^{\mathrm{meas}}|E_{\mathrm{jet},i}) \cdot W_\ell(E_\ell^{\mathrm{meas}}|E_\ell) \\ & \times W_{\mathrm{miss}}(E_x^{\mathrm{miss}}|p_x^\nu) \cdot W_{\mathrm{miss}}(E_y^{\mathrm{miss}}|p_y^\nu) \\ & \times W_\nu\left(\sqrt{(E_x^{\mathrm{miss}})^2+(E_y^{\mathrm{miss}})^2}|p_z^\nu\right). \end{aligned}$$

Other than expected, the neutrino efficiency dropped by about 5 % by this measure as shown in Fig. 5.14 for the electron sample. Also all other efficiencies decreased so that for improving efficiencies a transfer function for the neutrino p_z is not a good measure. The identification of the exact linear fit parameters was only performed for the electron sample. Because this result was very distinct, the process was not repeated separately for the muon sample.

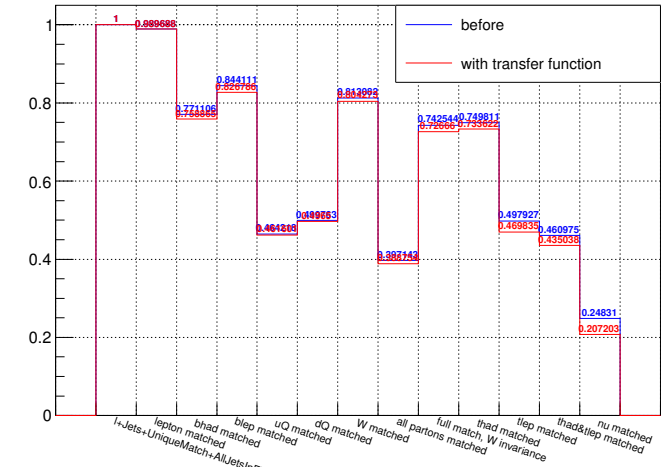

(a) Reconstruction efficiencies.

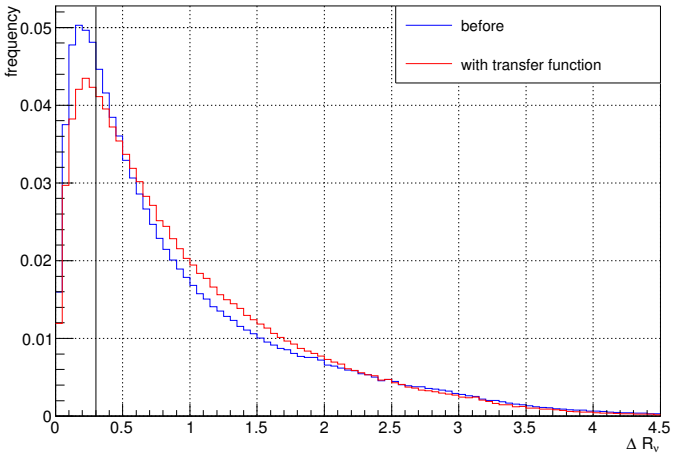

(b) ΔR distribution for the neutrino.

Figure 5.14.: Reconstruction performance as influenced by the implementation of a transfer function for the neutrino p_z for the electron sample.

6. Conclusion and Outlook

In summary, first, the values in the MatchMonster framework that define the reconstructed neutrino were changed to the fitted values instead of E_x^{miss}, E_y^{miss} and the calculated p_z^{ν}. With this, the quality of the KLFitter output got better because now the better matching momentum vector is compared to the true one of the decay particle.

Second, the starting value of the fitting process in KLFitter was changed. Instead of setting it to zero if the quadratic equation has no real solution, it is now set to the real part of the two complex solutions.

It was checked if in the case of two solutions of the quadratic equation the better one of the two solutions is chosen, which is the case. Last, an attempt to implement transfer functions for the p_z of the neutrino was made. But because the reconstruction efficiency worsened, this approach was not pursued.

In Fig. 6.1, the improvements accomplished by the work for this thesis are visible. The exact reconstruction efficiency values are listed in Table 6.1. The neutrino reconstruction efficiency could be raised by 3.04 % for the muon sample and by 2.83 % for the electron sample (see Table B.3). Also the reconstruction of all other particles could be improved as well by up to 4.92 % for the muon sample and up to 4.19 % for the electron sample.

Matching	Before Efficiency [%]	After Efficiency [%]
Muon	98.85	98.85
Leptonic b	84.21	84.35
Hadronic b	76.97	77.07
All partons	39.56	39.63
Hadronic t	74.50	74.63
Leptonic t	44.87	49.79
Neutrino ν	21.57	24.61

Table 6.1.: Selected reconstruction efficiencies before starting the studies and after adding all improvements in the program code.

Still, the value of the neutrino reconstruction efficiency is not as high as it was expected to be at the beginning of this thesis. For that reason, it can possibly be raised in future research. Studying η and ϕ further is a first suggestion for this.

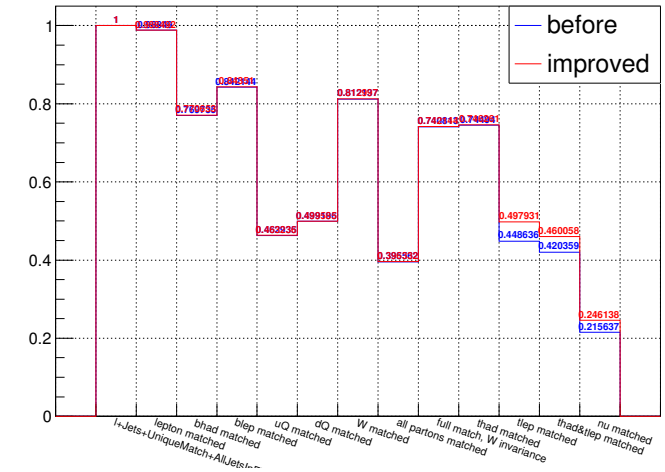

(a) reconstruction efficiencies.

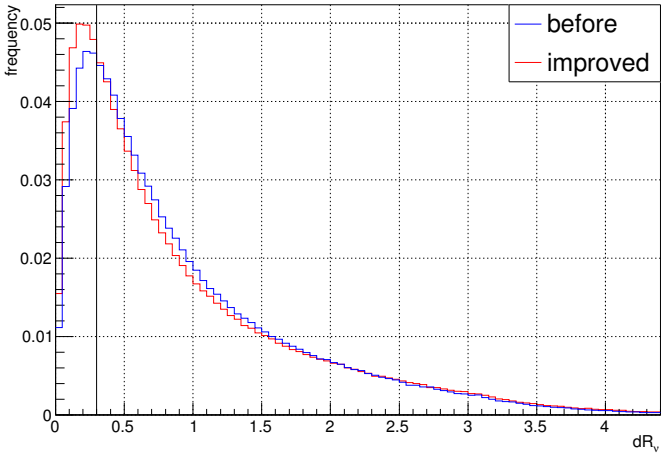

(b) ΔR distribution for the neutrino.

Figure 6.1.: Summary of all improvements in the reconstruction efficiencies of KLFitter.

Also, the separation in no and two solutions of the quadratic equation is important for continuing studies. As visible in Fig. 6.2, both cases behave differently. For no solution (Fig. 6.2(a)) the distribution of differences is almost equally bad for every value of p_z^{true}. The cluster around $p_z^{\text{true}} = 0$ is easily explained by the distribution of p_z^{true} (see Fig. 5.12) that peaks at the value of zero and follows approximately a double Gaussian function. So if there are more events at this value, it is also more likely that p_z^{reco} of more events equals p_z^{true}. Independently of the value of p_z^{true}, there is a slight indication of a piled appearance of $p_z^{\text{reco}} = 0$ because of the situation of the approximated ellipse around the origin of the plot.

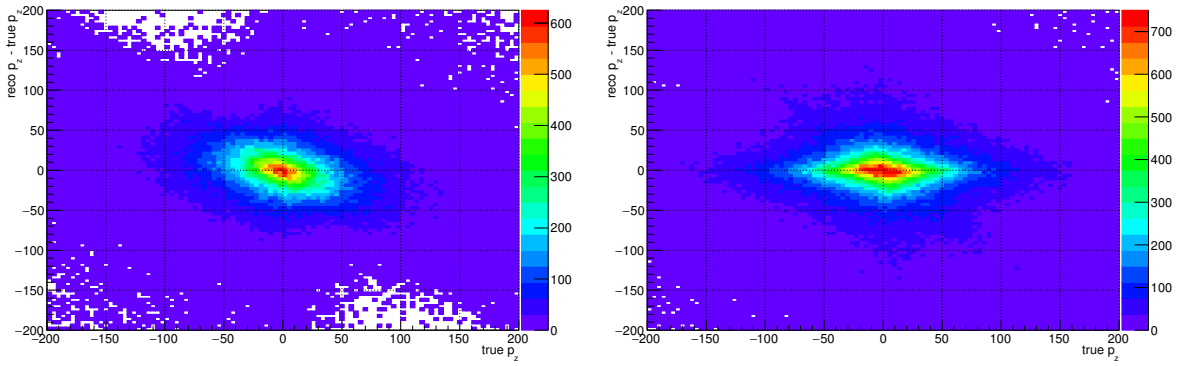

(a) Zero Solutions.

(b) Two Solutions.

Figure 6.2.: Difference between the reconstructed and true value in dependency on the true value of p_z of the neutrino separately for no and two solutions of the quadratic equation.

Things look very different for the two solution case in Fig. 6.2(b). Here, a lot more often the reconstruction worked and the difference plotted on the y-axis is zero. This fact is also independent of the value of p_z^{true} if one compares the distribution with the distribution of p_z^{true} in Fig. 5.12. As in the no solution case also $p_z^{\text{reco}} = 0$ happens often if the true value is not zero. But here, also another phenomenon is apparent. If the true value is zero itself, KLFitter often does not reconstruct it as zero but as a significant value. This circumstance is also already visible in Fig. 5.8.

The last observation is contradictory to an often reconstructed value of zero. If an implementation makes the reconstruction of zero less frequent, it simultaneously supports the other problem that $p_z^{\text{true}} = 0$ is less often reconstructed correctly.

This may be a reason for the still not very high reconstruction efficiency of the neutrino and the aggravation by the implementation of a new transfer function. It could also impede future studies in attempts on improving the efficiency further.

As desired, the neutrino reconstruction mechanism in KLFitter was investigated and locations of possible improvements were found. The goal to raise the reconstruction efficiency for the neutrino was reached with an increase of about 3 %.

A. Additional Plots

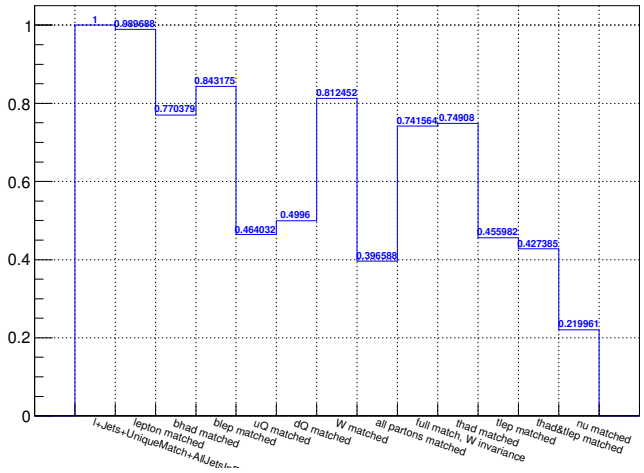

(a) Reconstruction efficiencies.

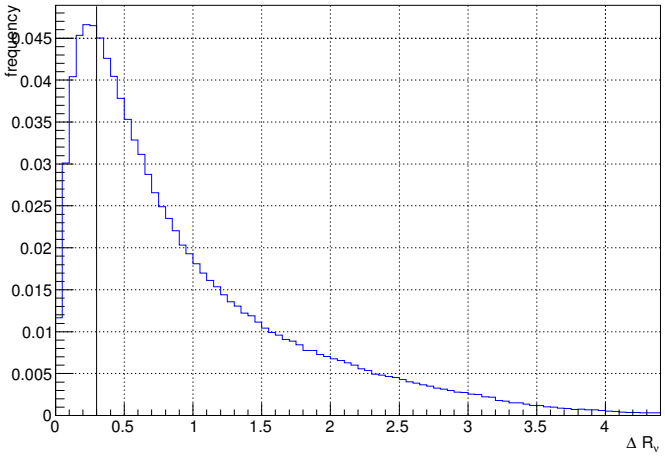

(b) ΔR distribution for the neutrino.

Figure A.1.: Status of the reconstruction efficiency before the analysis for the electron sample. At the top are the efficiencies of all regarded particles and at the bottom is the distribution of ΔR for the neutrino.

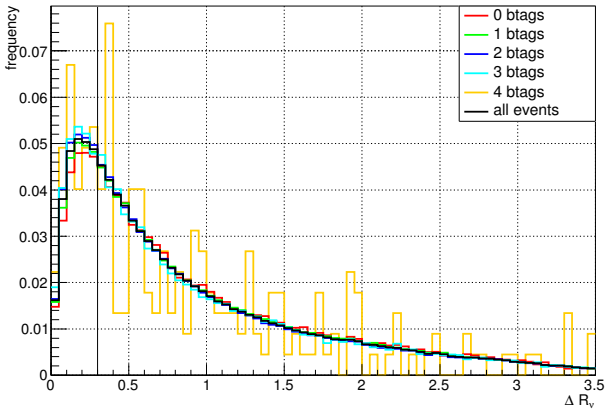

(a) b-Tags cut.

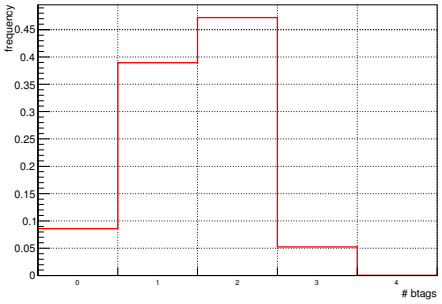

(b) b-Tags distribution.

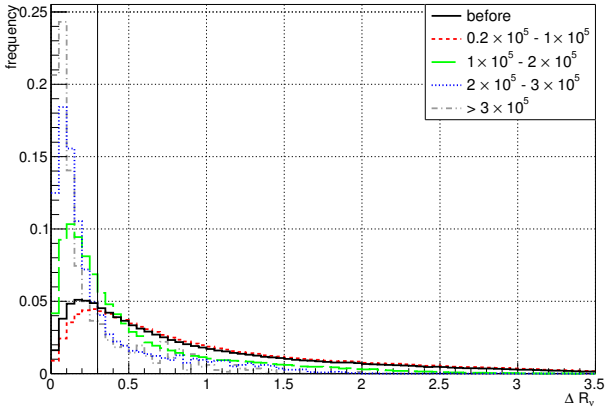

(c) $E_{\mathrm{T}}^{\mathrm{miss}}$ cut.

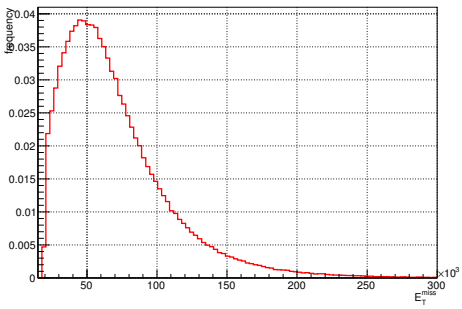

(d) $E_{\mathrm{T}}^{\mathrm{miss}}$ distribution.

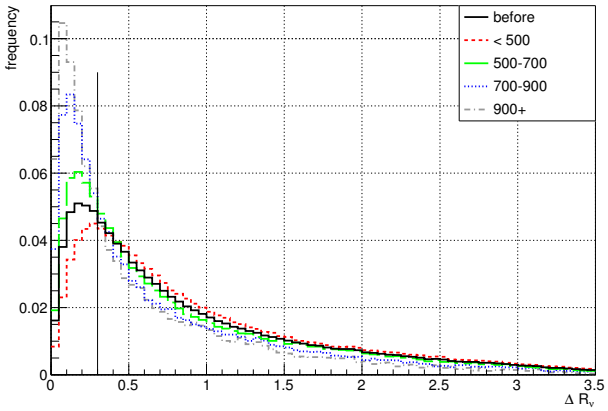

(e) $m_{t\bar{t}}$ cut.

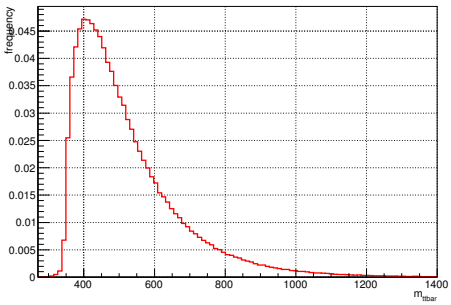

(f) $m_{t\bar{t}}$ distribution.

Figure A.2.: On the right side are the distributions of the possible cut parameters in the analysed electron sample. On the left side is the ΔR distribution for various ranges of possible cut parameters in analyses for the electron sample. The fraction of events that are below $\Delta R = 0.3$ increases with the number of b-tags, higher $E_{\mathrm{T}}^{\mathrm{miss}}$ and higher $m_{t\bar{t}}$. For these plots, the output files after all improvements in the code were used.

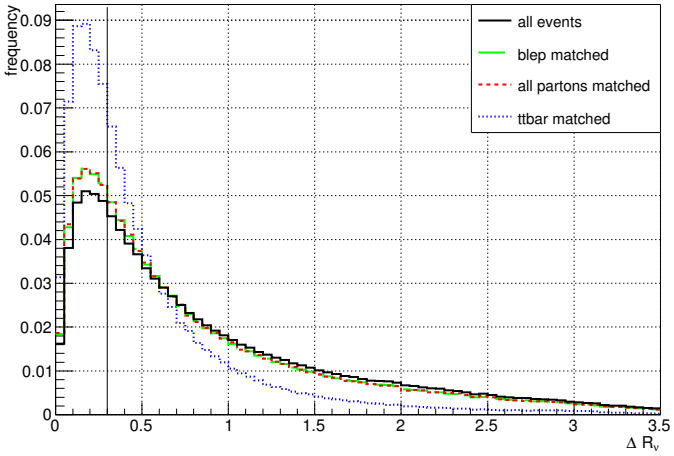

Figure A.3.: Distribution of ΔR for the neutrino for correctly reconstructed leptonic b-quark, all partons and the whole $t\bar{t}$ system for the electron sample. The first is fulfilled by about 84.41 %, the second by about 39.71 % and the latter by about 46.10 %. The first increases the reconstruction efficiency for the neutrino by about 3.08 %, the second by about 3.14 % and the latter by about 19.11 %. For this plot, the output files after all improvements in the codes were used.

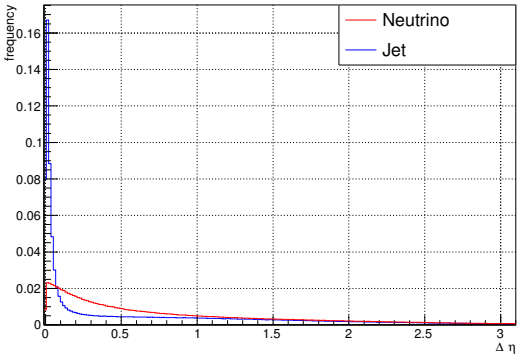

(a) $\Delta\eta$ for $\mu+$jets.

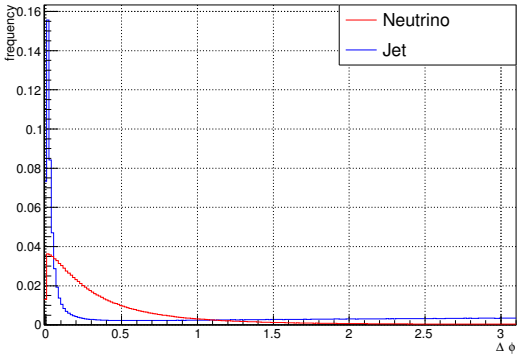

(b) $\Delta\phi$ for $\mu+$jets.

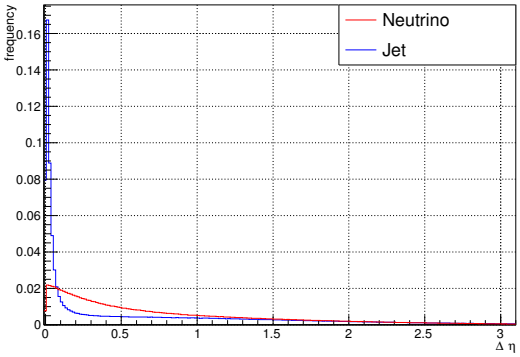

(c) $\Delta\eta$ for $e+$jets.

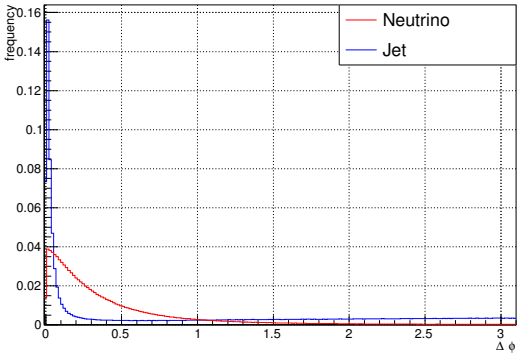

(d) $\Delta\phi$ for $e+$jets.

Figure A.4.: The difference between the true and the reconstructed entries of η and ϕ are compared for the neutrino and a jet. Here as jet the hadronic b-jet is chosen since it has less decay correlation with the neutrino than the leptonic b but a better reconstruction efficiency than the light quarks.

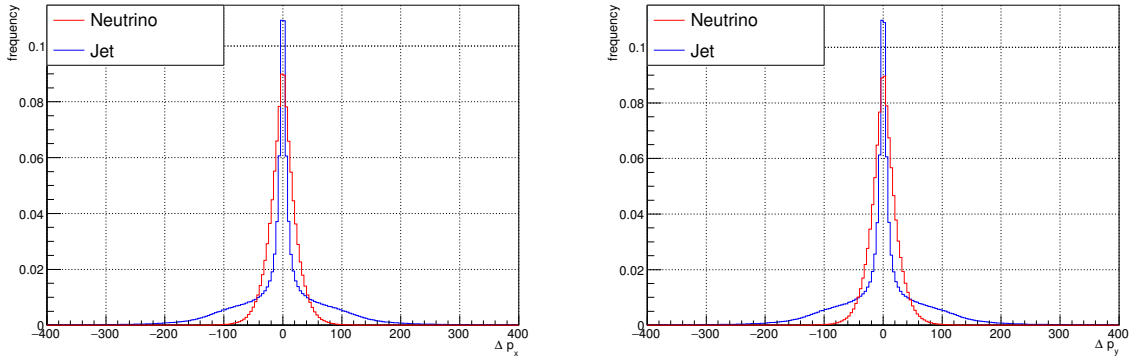

(a) Δp_x.

(b) Δp_y.

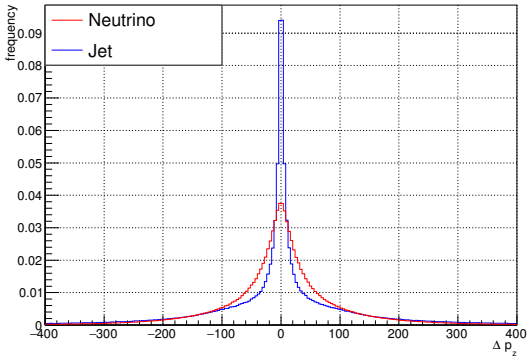

(c) Δp_z.

Figure A.5.: The difference between the true and the reconstructed entries of the momentum vector is compared for the neutrino and a jet for the electron sample. Here as jet the hadronic b-jet is chosen since it has less decay correlation with the neutrino than the leptonic b but a better reconstruction efficiency than the light quarks.

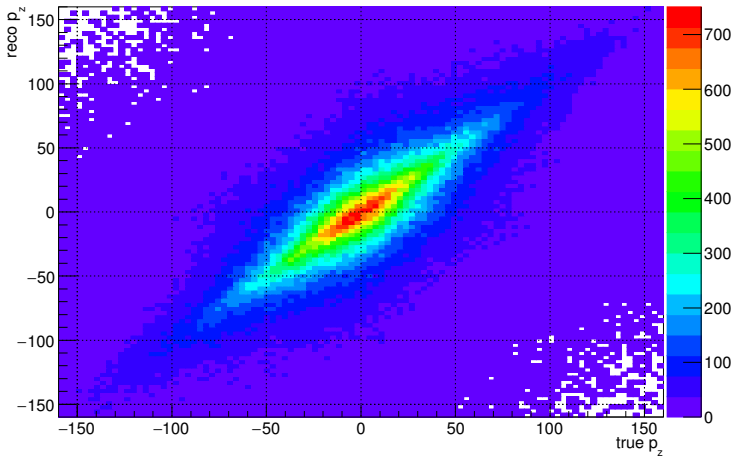

Figure A.6.: Distribution of p_z^{reco} to p_z^{true} for the neutrino in the electron sample in the analysed data.

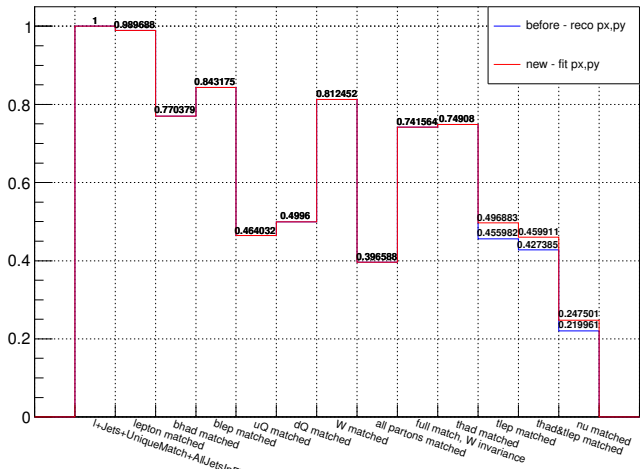

(a) Reconstruction efficiencies.

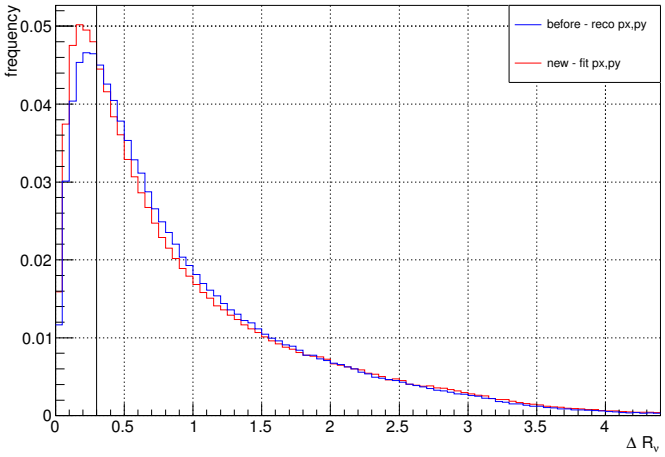

(b) ΔR distribution for the neutrino.

Figure A.7.: Status of the reconstruction efficiency for the electron sample after improving the MatchMonster framework. At the top are the efficiencies of all regarded particles and at the bottom is the distribution of ΔR for the neutrino.

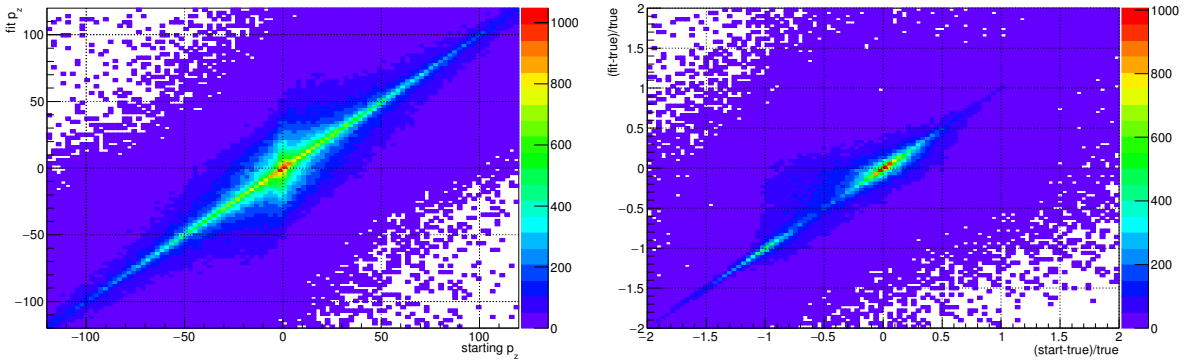

(a) Fitted p_z vs. starting p_z.

(b) Deviation of fitted p_z vs. deviation of starting p_z scaled to units of p_z^{true}.

Figure A.8.: Studies on the dependencies of the fitted neutrino p_z value on the starting value of the fit for the electron sample. The fitted value is highly dependent on the value the fit starts with.

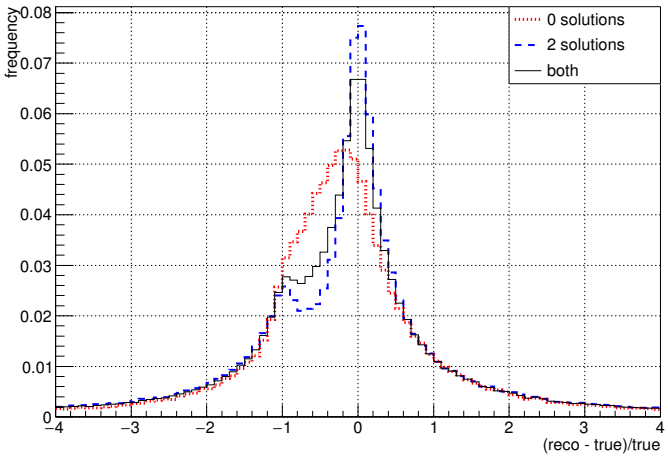

Figure A.9.: Distribution of Δp_z scaled to p_z^{true} plotted against the p_z^{true} value for the neutrino in the electron sample.

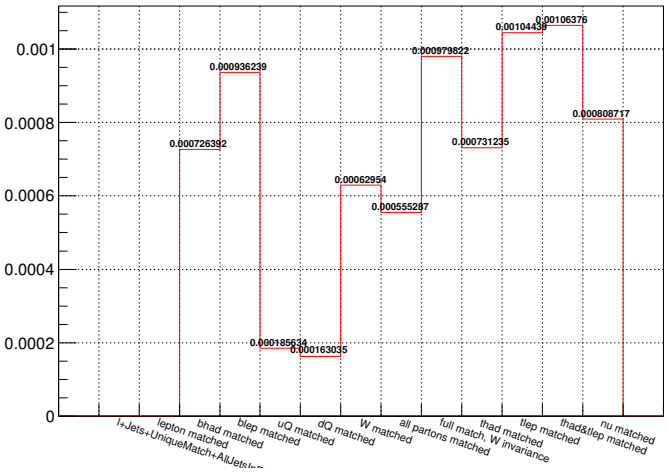

(a) Difference in the reconstruction efficiencies.

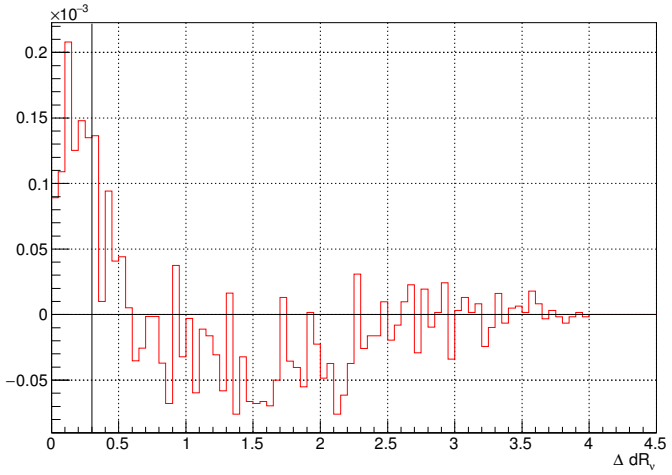

(b) Difference in the ΔR distribution for the neutrino.

Figure A.10.: Differences in reconstruction efficiencies in the electron sample between the improved KLFitter framework after implementing the new zero solution starting value and the before status.

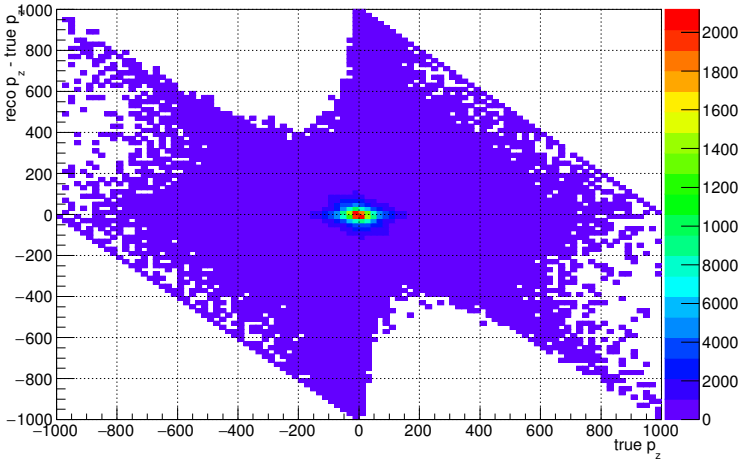

Figure A.11.: The spreading of the difference between p_z^{reco} and p_z^{true} in dependency on p_z^{true} for the neutrino in the electron sample.

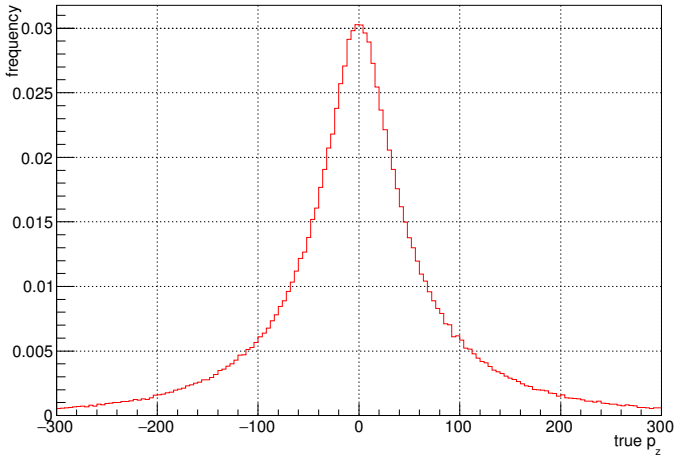

Figure A.12.: Distribution of p_z^{true} of the neutrino in the used Monte Carlo samples for the $e+\text{jets}$ channel.

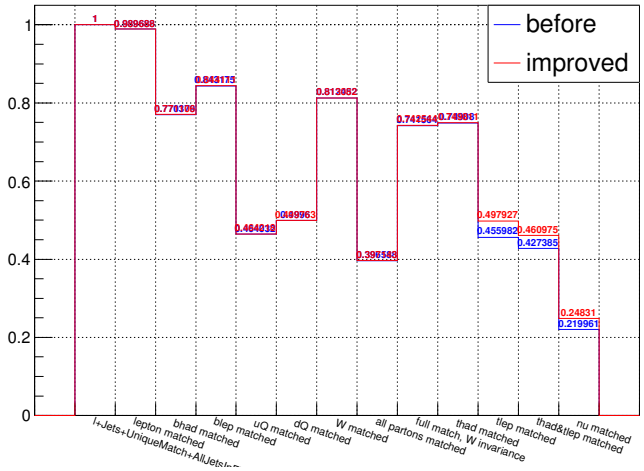

(a) Reconstruction efficiencies.

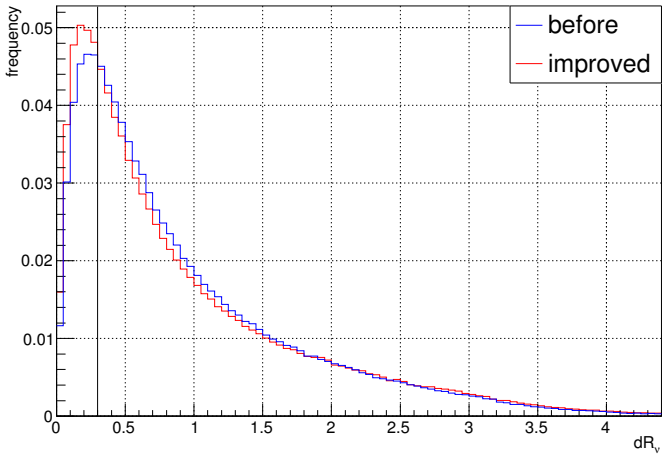

(b) ΔR distribution for the neutrino.

Figure A.13.: Summary of all improvements in the reconstruction efficiencies of KLFitter for the electron sample.

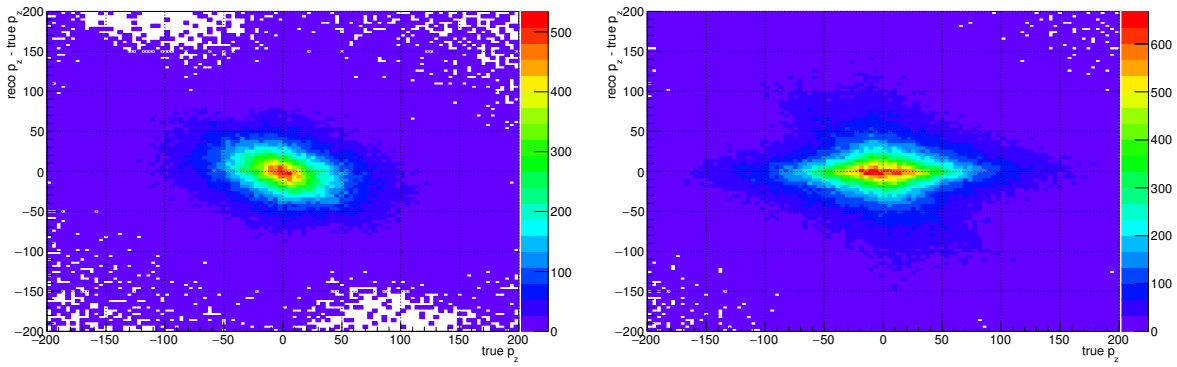

(a) Zero Solutions.

(b) Two Solutions.

Figure A.14.: The spreading of the difference between p_z^{reco} and p_z^{true} in dependency on p_z^{true} for the neutrino in the electron sample.

B. Additional Tables

Matching	Efficiency [%]
Electron	98.97
Leptonic b	84.32
Hadronic b	77.04
All partons	39.66
Hadronic t	74.91
Leptonic t	45.60
Neutrino ν	22.00

Table B.1.: Reconstruction efficiencies of important decay particles in the $e+$jets channel before the analysis as shown in Fig. A.1(a).

Cut Parameter	Improvement [%]	Remaining Statistics [%]
At least one b-tag	0.17	91.42
At least two b-tags	0.74	52.46
At least three b-tags	1.13	5.27
Four b-tags	2.84	0.04
$E_T^{\text{miss}} > 50,000\,\text{GeV}$	6.96	65.34
$E_T^{\text{miss}} > 100,000\,\text{GeV}$	24.51	17.87
$E_T^{\text{miss}} > 150,000\,\text{GeV}$	37.82	4.67
$E_T^{\text{miss}} > 200,000\,\text{GeV}$	44.46	1.33
$m_{t\bar{t}} > 400\,\text{GeV}/c^2$	2.02	81.83
$m_{t\bar{t}} > 500\,\text{GeV}/c^2$	7.18	44.69
$m_{t\bar{t}} > 600\,\text{GeV}/c^2$	11.95	22.78

Table B.2.: Improvement of the neutrino reconstruction efficiency and remaining statistics when performing special cuts on the used data for the electron sample. The improvement gives the value that needs to be added to the efficiency before performing the cut. The value in the column remaining statistics gives the percentage of the sample that is left for analysis after performing the cut.

Matching	Before Efficiency [%]	After Efficiency [%]
Electron	98.97	98.97
Leptonic b	84.32	84.42
Hadronic b	77.04	77.04
All partons	39.66	39.71
Hadronic t	74.91	74.98
Leptonic t	45.60	49.79
Neutrino ν	22.00	24.83

Table B.3.: Selected reconstruction efficiencies for the electron sample before this thesis and after improving several things in the program codes.

Bibliography

[1] S. L. Glashow, *Partial-symmetries of weak interactions*, Nucl. Phys. **22(4)**, 579 (1961)

[2] S. Weinberg, *A Model of Leptons*, Phys. Rev. Lett. **19**, 1264 (1967)

[3] S. L. Glashow, J. Iliopoulos, L. Maiani, *Weak Interactions with Lepton-Hadron Symmetry*, Phys. Rev. D **2**, 1285 (1970)

[4] H. Georgi, S. L. Glashow, *Unified Weak and Electromagnetic Interactions without Neutral Currents*, Phys. Rev. Lett. **28**, 1494 (1972)

[5] H. D. Politzer, *Reliable Perturbative Results for Strong Interactions?*, Phys. Rev. Lett. **30**, 1346 (1973)

[6] H. D. Politzer, *Asymptotic freedom: An approach to strong interactions*, Physics Reports **14** (1974)

[7] D. J. Gross, F. Wilczek, *Ultraviolet Behavior of Non-Abelian Gauge Theories*, Phys. Rev. Lett. **30**, 1343 (1973)

[8] S. Weinberg, *The making of the Standard Model*, Eur. Phys. J. C **34**, 5 (2004)

[9] G. 't Hooft, *Renormalizable Lagrangians for massive Yang-Mills fields*, Nucl. Phys. B **35** (1971)

[10] G. 't Hooft, M. Veltman, *Regularization and renormalization of gauge fields*, Nucl. Phys. B **44** (1972)

[11] G. 't Hooft, M. Veltman, *Combinatorics of gauge fields*, Nucl. Phys. B **50** (1972)

[12] ATLAS Collaboration, *Observation of a new particle in the search for the Standard Model Higgs boson with the ATLAS detector at the LHC*, Phys. Lett. B **716(1)**, 1 (2012)

[13] *Observation of a new boson at a mass of 125 GeV with the* CMS *experiment at the* LHC, Phys. Lett. B **716**, 30 (2012)

[14] D. J. Griffiths, *Introduction to Elementary Particles*, Wiley-VCH, 2nd edition (2012)

[15] B. Povh, et al., *Teilchen und Kerne, Eine Einführung in die physikalischen Konzepte*, Springer, 7th edition (2006)

[16] K. Olive, et al. (Particle Data Group), Chin. Phys. **C38**, 090001 (2014)

[17] F. Halzem, A. Martin, *Quarks and Leptons: An Introductory Course in Modern Particle Physics*, Wiley (1984)

[18] M. Kobayashi, T. Maskawa, *CP-Violation in the Renormalizable Theory of Weak Interaction*, Prog. Theor. Phys. **49**, 652 (1973)

[19] F. Abe, et al. (The CDF Collaboration), *Observation of Top Quark Production in $\overline{p}p$ Collisions with the Collider Detector at Fermilab*, Phys. Rev. Lett. **74**, 2626 (1995)

[20] S. Abachi, et al. (The DØ Collaboration), *Observation of the Top Quark*, Phys. Rev. Lett. **74**, 2632 (1995)

[21] T. Aaltonen, et al. (The CDF Collaboration), *Observation of Electroweak Single Top-Quark Production*, Phys. Rev. Lett. **103**, 092002 (2009)

[22] V. M. Abazov, et al. (The DØ Collaboration), *Observation of Single Top-Quark Production*, Phys. Rev. Lett. **103**, 092001 (2009)

[23] ATLAS Collaboration, CDF Collaboration, CMS Collaboration, DØ Collaboration, *First combination of* TEVATRON *and* LHC *measurements of the top-quark mass* (2014), aTLAS-CONF-2014-008, CDF-NOTE-11071, CMS-PAS-TOP-13-014, D0-NOTE-6416, `1403.4427`

[24] P. J. Mohr, B. N. Taylor, D. B. Newell, *CODATA Recommended Values of the Fundamental Physical Constants: 2010a)*, J. Phys. Chem. Ref. Data **41(4)**, 043109 (2012)

[25] D0 Collaboration, *Improved determination of the width of the top quark*, Phys. Rev. D **85**, 091 (2012)

[26] I. Bigi, et al., *Production and decay properties of ultra-heavy quarks*, Phys. Lett. B **181(1,2)**, 157 (1986)

[27] J. Pumplin, et al., *New Generation of Parton Distributions with Uncertainties from Global QCD Analysis*, JHEP **2002(07)**, 012 (2002)

[28] A. Quadt, *Top quark physics at hadron colliders*, Eur. Phys. J. C **48(3)**, 835 (2006)

[29] L. Evans, P. Bryant, *LHC Machine*, JINST **3(08)**, S08001 (2008)

[30] M. Capeans, et al., *ATLAS Insertable B-Layer Technical Design Report*, Technical Report CERN-LHCC-2010-013. ATLAS-TDR-19, CERN (2010)

[31] K. Aamodt, et al. (ALICE Collaboration), *The ALICE experiment at the CERN LHC*, JINST **3(08)**, S08002 (2008)

[32] A. Augusto Alves Jr., et al. (LHCb Collaboration), *The LHCb Detector at the LHC*, JINST **3(08)**, S08005 (2008)

[33] ATLAS Collaboration, *The ATLAS Experiment at the CERN Large Hadron Collider*, JINST **3(08)**, S08003 (2008)

[34] CMS Collaboration, *The CMS experiment at the CERN LHC*, JINST **3(08)**, S08004 (2008)

[35] J. Pinfold, et al. (MoEDAL Collaboration), *Technical Design Report of the MoEDAL Experiment*, Technical Report CERN-LHCC-2009-006. MoEDAL-TDR-001, CERN (2009)

[36] V. Berardi, et al. (TOTEM Collaboration), *TOTEM: Technical design report. Total cross section, elastic scattering and diffraction dissociation at the Large Hadron Collider at CERN*, Technical Report CERN-LHCC-2004-002, TOTEM-TDR-001, CERN (2004)

[37] ATLAS Collaboration, *Performance of the ATLAS Inner Detector Track and Vertex Reconstruction in the High Pile-Up LHC Environment*, Technical Report ATLAS-CONF-2012-042, CERN (2012)

[38] J. Erdmann, et al., *A likelihood-based reconstruction algorithm for top-quark pairs and the KLFitter framework*, Nucl. Instrum. Meth. **A748**, 18 (2014)

[39] A. Caldwell, D. Kollár, K. Kröninger, *BAT - The Bayesian analysis toolkit*, Comput. Phys. Commun. **180(11)**, 2197 (2009)

[40] T. Sjöstrand, S. Mrenna, P. Skands, *PYTHIA 6.4 physics and manual*, JHEP **2006(05)**, 026 (2006)

[41] S. Frixione, P. Nason, C. Oleari, *Matching NLO QCD computations with parton shower simulations: the POWHEG method*, JHEP **2007(11)**, 070 (2007)

[42] P. Calafiura, et al., *The athena control framework in production, new developments and lessons learned*, in *Computing in high energy physics and nuclear physics. Proceedings Conference, CHEP'04, Interlaken, Switzerland, September 27-October 1, 2004*, page 456 (2005)

[43] G. Soyez, *The SISCone and anti-k(t) jet algorithms*, in *Proceedings, 16th International Workshop on Deep Inelastic Scattering and Related Subjects (DIS 2008)*, page 178 (2008)

[44] ATLAS Collaboration, *Measurement of the $t\bar{t}$ production cross-section using $e\mu$ events with b-tagged jets in pp collisions at $\sqrt{s} = 7$ and 8 TeV with the ATLAS detector*, Eur. Phys. J. C **74(10)**, 3109 (2014)

[45] ATLAS Collaboration, *Measurements of spin correlation in top-antitop quark events from proton-proton collisions at $\sqrt{s} = 7$ TeV using the ATLAS detector*, Phys. Rev. D **90**, 112016 (2014)

[46] ATLAS Collaboration, *Measurements of normalized differential cross sections for $t\bar{t}$ production in pp collisions at $\sqrt{(s)} = 7$ TeV using the ATLAS detector*, Phys. Rev. D **90**, 072004 (2014)

Acknowledgements

First of all I want to thank Prof. Dr. Arnulf Quadt for the opportunity to write my bachelor's thesis in his department under his supervision and also for being my first referee. Second my gratitude goes to Prof. Dr. Ariane Frey for her willingness to be the second referee.

I am very grateful to Dr. Boris Lemmer, who supported my work in a committed way, answered all my questions and did not get tired of explaining how KLFitter works. Sincere thanks to Philipp Stolte for the same amount of support in working and writing, especially for providing me with the Monte Carlo samples and fixing all GRID and ROOT related problems. Also my honest gratitude to the two of them for proof-reading this thesis and being ready to help at any time.

In this context I would like to acknowledge the participation of the II. Physikalisches Institut in Göttingen (and especially Prof. Dr. Arnulf Quadt) in representing particle physics at many opportunities to students in the form of the IdeenExpo, particle physics masterclasses, public talks and so on. My enthusiasm for particle physics got kindled by this while I was forced to complete school first before beginning to study. Also thanks to the Netzwerk Teilchenwelt for making this waiting bearable when I got the chance to visit a workshop for students at CERN.

A special thanks to my parents who always encouraged me to learn new things and dragged me to every science related museum or event in sight when I was a child. It finally paid off.

Erklärung nach §13(9) der Prüfungsordnung für den Bachelor-Studiengang Physik und den Master-Studiengang Physik an der Universität Göttingen:

Hiermit erkläre ich, dass ich diese Abschlussarbeit selbständig verfasst habe, keine anderen als die angegebenen Quellen und Hilfsmittel benutzt habe und alle Stellen, die wörtlich oder sinngemäß aus veröffentlichten Schriften entnommen wurden, als solche kenntlich gemacht habe.
Darüberhinaus erkläre ich, dass diese Abschlussarbeit nicht, auch nicht auszugsweise, im Rahmen einer nichtbestandenen Prüfung an dieser oder einer anderen Hochschule eingereicht wurde.

Göttingen, den 23. Juni 2016

(Marie Reinecke)